Published for SISSA by Springer

Received: April 28, 2023
Revised: July 24, 2023
Accepted: August 18, 2023
Published: August 29, 2023

Primordial black hole archaeology with gravitational waves from cosmic strings

Anish Ghoshal,[a] Yann Gouttenoire,[b] Lucien Heurtier[c] and Peera Simakachorn[d]

[a] *Institute of Theoretical Physics, Faculty of Physics, University of Warsaw, ul. Pasteura 5, 02-093 Warsaw, Poland*

[b] *School of Physics and Astronomy, Tel-Aviv University, Tel-Aviv 69978, Israel*

[c] *Institute for Particle Physics Phenomenology, Durham University, South Road, Durham, U.K.*

[d] *Instituto de Física Corpuscular (IFIC), Universitat de València-CSIC, C/ Catedrático José Beltrán 2, E-46980, Paterna, Spain*

E-mail: anish.ghoshal@fuw.edu.pl, yann.gouttenoire@gmail.com, lucien.heurtier@durham.ac.uk, peera.simakachorn@ific.uv.es

Abstract: Light primordial black holes (PBHs) with masses smaller than 10^9 g ($10^{-24} M_\odot$) evaporate before the onset of Big-Bang nucleosynthesis, rendering their detection rather challenging. If efficiently produced, they may have dominated the universe energy density. We study how such an early matter-dominated era can be probed successfully using gravitational waves (GW) emitted by local and global cosmic strings. While previous studies showed that a matter era generates a single-step suppression of the GW spectrum, we instead find a *double-step* suppression for local-string GW whose spectral shape provides information on the duration of the matter era. The presence of the two steps in the GW spectrum originates from GW being produced through two events separated in time: loop formation and loop decay, taking place either before or after the matter era. The second step — called the *knee* — is a novel feature which is universal to any early matter-dominated era and is not only specific to PBHs. Detecting GWs from cosmic strings with LISA, ET, or BBO would set constraints on PBHs with masses between 10^6 and 10^9 g for local strings with tension $G\mu = 10^{-11}$, and PBHs masses between 10^4 and 10^9 g for global strings with symmetry-breaking scale $\eta = 10^{15}$ GeV. Effects from the spin of PBHs are discussed.

Keywords: Cosmology of Theories BSM, Early Universe Particle Physics, Phase Transitions in the Early Universe, Specific BSM Phenomenology

ArXiv ePrint: 2304.04793

https://doi.org/10.1007/JHEP08(2023)196

JHEP08(2023)196

Contents

1 Introduction

The precise measurement of the Cosmic Microwave Background (CMB) [1] and the successful prediction of Big-Bang Nucleosynthesis (BBN) [2–4] have determined the amount of radiation, baryons, dark matter and dark energy in our universe with extraordinary accuracy. Temperature anisotropies measured in the CMB superimposed on the perfectly smooth background suggest that our universe has started with an accelerated expansion called cosmic inflation [5–8]. However, the cosmic history after inflation and before BBN — above the plasma temperature of $T \gtrsim 1$ MeV — is difficult to probe and is currently unconstrained by data. The standard assumption that the pre-BBN universe is radiation-dominated might be challenged by open problems in the Standard Model (SM) of particle physics, e.g., the origin of the matter-antimatter asymmetry, the origin of dark matter, the flavor puzzle, or the ultraviolet dynamics in the Higgs sector, see e.g. ref. [9] for a review. New physics addressing those issues requires the introduction of new energy scales and new degrees of freedom, which sometimes generate deviations from the standard radiation domination era before the onset of BBN. Well-known examples are a long-lived heavy scalar field generating an early matter era [10–17], a fast-moving scalar field generating a kination era [18–26], or a supercooled phase transition [27–39]. In the present work, we are interested in the possibility that the early universe underwent a matter-dominated phase induced by a population of Primordial Black Holes (PBHs) evaporating before BBN.[1]

Unlike astrophysical black holes, PBHs can have masses that range from $M_{\rm PBH} \lesssim 0.1$ g to 10^{23} g [43, 44]. They originate from the collapse of primordial curvature over-densities [45]. Such primordial inhomogeneities can be sourced by cosmic inflation [46, 47], transitions to a metastable vacuum during inflation [48–51], supercooled phase transitions [52–60], bubble collisions [61–64], matter squeezing by bubble walls [65–68], collapse of scalar condensate [69–74], of domain walls [75–79], or of cosmic-string loops [80–87]. PBHs lighter than 10^{15} g would have already evaporated by now [88, 89]. The ones in the range $10^9\ {\rm g} \lesssim M_{\rm PBH} \lesssim 10^{15}$ g would have evaporated after the onset of BBN and are strongly constrained by cosmological observations [90, 91]. However, PBHs lighter than 10^9 g evaporate in the pre-BBN universe, and their observational signatures are considerably limited.

The detection of gravitational waves (GWs) from astrophysical sources by the LIGO-Virgo collaboration in 2015 [92] opened the door to GW astronomy. Upcoming upgrades of LIGO-Virgo [93] and proposed future detectors such as LISA [94], BBO-DECIGO [95], the Einstein Telescope (ET) [96, 97], and Cosmic Explorer (CE) [98] will open up a new observation window of the early universe. Unlike photons, primordial GWs that were emitted in the early Universe can propagate freely throughout cosmic history and therefore would constitute ideal messengers of our Universe history [99–101]. One of the pinnacles for determining the pre-BBN cosmic history of the universe would be the detection of GW sourced by a network of cosmic strings. Cosmic strings are one-dimensional objects produced by the spontaneous breaking of a U(1) symmetry in the early universe [102, 103], the pure Yang-Mills theory [104, 105], or fundamental objects in superstring theory [106–110]. The crucial peculiarity of cosmic strings is that they are long-standing GW sources [111–114]. Once the network of cosmic strings is produced, it occupies a constant fraction of the total energy density of the universe, a property known as the scaling regime [115–120]. An important consequence is that GW emissions occur during most of the universe history. This generates a GW spectrum spanning many orders of magnitude in frequencies. A mea-

[1]Early eras of cosmology deviating from radiation domination may also arise when an extended particle physics sector or an extended distribution of PBHs decays/evaporate in the early universe, as studied in refs. [40–42].

JHEP08(2023)196

surement of the GW spectrum from high to lower frequencies would allow to determine the universe expansion rate from early to later times [16, 121–128]. Instead, the use of short-lived GW sources like the ones from first-order phase transitions can only probe the cosmic history within a small window of time around when the source is active [22, 129–132]. Another long-standing GW source that could bring information about the equation of state of the pre-BBN universe is tensor modes sourced during primordial inflation [133–137]. The BICEP-Keck bound on the tensor-to-scalar ratio $r \lesssim 0.036$ [138] constrains the inflation scale to $H_{\rm inf} \lesssim 3 \times 10^{13}$ GeV which prevents the detectability of tensor modes by GW detectors in a foreseeable future [139–142]. However, intermediate cosmological eras can imprint signatures on such GW spectrum [22, 23, 143–146].

In this work, we explore how a period of early matter domination that originates from a large production of PBHs in the early Universe could leave observable imprints in the spectrum of GWs generated by a network of cosmic strings. We do not assume any connection between the sector producing PBHs and the one producing cosmic strings. *The paper is organized as follows:* in section 2, we review the calculation of the GW spectrum from cosmic strings, both in the local and global cases, as illustrated in figure 1. Readers familiar with cosmic strings can jump directly to section 3 where we study the impact of a matter-dominated era. The main smoking-gun GW signatures are summarized in figure 2, including the *double-step* feature and its associated *knee*, which are studied for the first time in this work. Finally, in section 4, we use those findings to constrain the abundance and mass of primordial black holes formed with a monochromatic distribution, see figure 6 and 7 for local and global strings, respectively. We would like to emphasize that the PBHs considered in this work evaporated well before BBN. Hence the constraints are shown as the fraction of energy density β in PBH at formation, instead of today PBH fraction $\Omega_{\rm PBH}$. We discuss these results and conclude in section 5.

2 GW from cosmic strings

A cosmological phase transition associated with the spontaneous breaking of U(1) symmetry leads to the formation of a network of topological defects called *cosmic strings* (CS). The U(1) symmetry can be either *local* or *global*. We refer to ref. [103] for the original article, ref. [114] for a textbook, and refs. [9, 101, 124, 147, 148] for reviews of their GW emission.

Cosmic strings are field configurations at the top of the U(1)-breaking Mexican hat potential. The field energy is localized within a core of inverse symmetry-breaking scale size, much smaller than the cosmological horizon. This motivates the *Nambu-Goto* approximation which describes CS as infinitely thin classical objects with energy per unit length μ,

$$\mu = 2\pi n\, \eta^2 \times \begin{cases} 1 & \text{for local strings,} \\ \log(\eta t) & \text{for global strings,} \end{cases} \tag{2.1}$$

where η is the vacuum expectation value of the scalar field constituting CS, and n is the winding number taken to be $n = 1$ since it is the only stable configuration [149]. For global

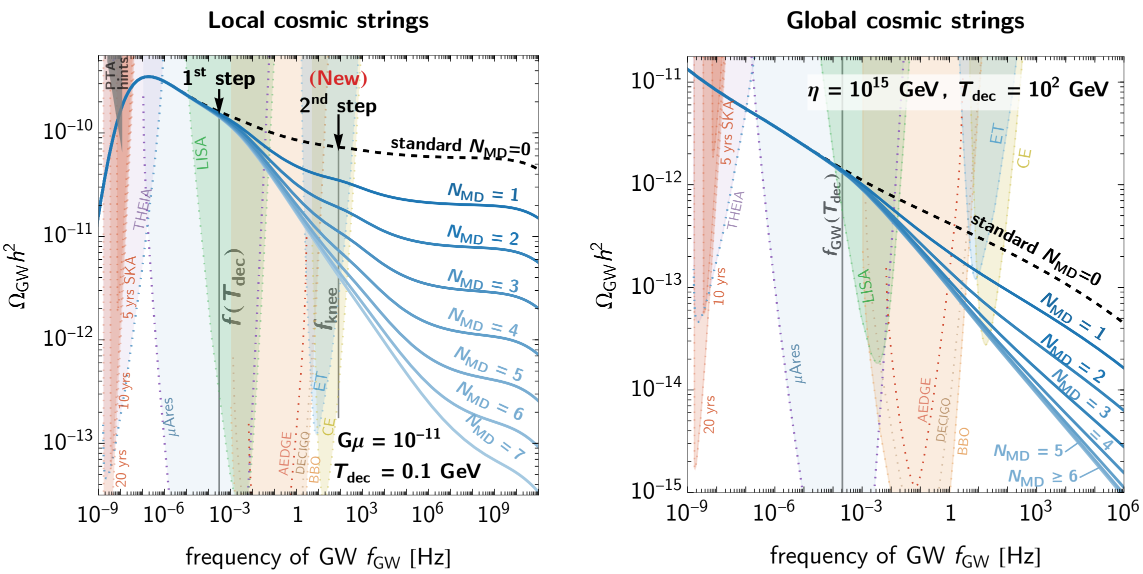

Figure 1. We assume an early matter domination (e.g., PBH domination era) lasting for $N_{\rm MD}$ e-folds of Hubble expansion and ending at temperature $T_{\rm dec}$. It impacts the GW spectra of local and global cosmic strings through a double-step (**left**) and a single-step (**right**) suppression, respectively. Those features can be characterized by three frequencies: the low-frequency turning point, the high-frequency plateau, and the newly-found knee (the second step in local strings GW spectrum), see section 3.

strings, the logarithmic divergence arises due to the massless Goldstone mode leading to the presence of long-range gradient energy [114]. The CS network forms at the temperature of the U(1)-breaking phase transition,

$$T_{\rm form} \simeq \eta \simeq 10^{11}\ {\rm GeV} \left(\frac{G\mu}{10^{-15}}\right)^{1/2}, \tag{2.2}$$

where the second equality refers to local strings.

2.1 Evolution of the network

In general, one should expect the motion of cosmic strings to be initially frozen due to thermal friction, characterized by the frictional damping length $l_f = \mu/(\beta T^3)$ where $\beta = \mathcal{O}(1)$ represents the strength of particle-string interactions [150–152]. At that time the energy density of frozen CS evolves under Hubble expansion as $\rho_{\rm CS} \propto a^{-2}$ where a is the scale factor [114], and would quickly dominate the energy density of the universe. Effects from friction become negligible when the damping length l_f becomes larger than the cosmic horizon t, i.e., when

$$T \lesssim T_{\rm fric} = \frac{4\times 10^9\ {\rm GeV}}{\beta}\left(\frac{g_*}{100}\right)^{1/2}\left(\frac{G\mu}{10^{-11}}\right). \tag{2.3}$$

Below that temperature, CS start to move freely under the work of their own tension, they reach velocities of order $\mathcal{O}(0.1)$ and start to interact with each other [114]. The intersection

JHEP08(2023)196

of straight strings forms loops that decay by radiating particles and GW. Loop formation acts as a loss mechanism for the infinitely long-string network. Out of those two antagonist effects, Hubble expansion and loop formation, which respectively increase and decrease the fractional CS abundance $\Omega_{\rm CS} \equiv \rho_{\rm CS}/\rho_{\rm tot}$, the CS network reaches a stable state called the *scaling regime* where $\Omega_{\rm CS}$ remains constant over time [115–120]. In the scaling regime, CS redshifts the same way as the background, e.g., $\rho_{\rm CS} \propto a^{-4}$ during radiation-domination (RD) and $\rho_{\rm CS} \propto a^{-3}$ during matter-domination (MD). One can say that the equation of state of the CS network tracks the equation of state of the expanding background.

The GW signal from CS is dominated by emission from loops [112, 114, 153]. Loops of strings are constantly being produced as long strings self-intersect. Local string loops decay into GW after $0.001/G\mu \gg 1$ Hubble time, while global string loops decay into Goldstone modes in less than one Hubble time, cf. eq. (2.16).

- **Step 1: Loop Formation.** We denote α the size of loops in units of the cosmic horizon t_i when they form. The rate of loop formation rate can be written [114]

$$\frac{dn_{\rm loop}}{dt_i} = 0.1\frac{C_{\rm eff}(t_i)}{\alpha t_i^4}, \tag{2.4}$$

  where factor 0.1 indicates that 90% of the loop population is small and highly-boosted loops that are red-shifted away and do not contribute substantially to the GW signal [154]. We have introduced the loop formation efficiency factor $C_{\rm eff}$, which for local strings reaches the asymptotic value $C_{\rm eff} \simeq 0.39$, 5.4, 29.6 during matter-domination (MD), radiation-domination (RD), and kination eras, respectively [124]. For global strings, the long strings lose energy via Goldstone emission on top of loop formation, which logarithmically suppresses the loop production efficiency. At the analytical level, we take $C_{\rm eff} \sim \mathcal{O}(1)$ for all cosmological eras [124, 155, 156]. However, for the plots and analysis of this paper, we solve $C_{\rm eff}(t)$ as a solution of the velocity-dependent one-scale (VOS) equations governing the string network evolution. As studied thoroughly in refs. [124, 157], the VOS evolution captures the inertia of the network during a change in the equation of state of the universe. Instead, approximating $C_{\rm eff}$ using a piecewise constant function across different eras overestimates the value of the turning-point frequency in eq. (2.17) by more than one order of magnitude [124].

- **Step 2: GW Emission from Loops.** Numerical simulations [154] have shown that the GW spectrum is dominantly produced by loops with the largest size, corresponding to 10% of the horizon. We account for this result by choosing a monochromatic loop size probability distribution

$$\mathcal{P}_{\rm loop}(\alpha) = \delta(\alpha - 0.1). \tag{2.5}$$

  After their formation, $\tilde{t} > t_i$, loops of length $l(\tilde{t})$ oscillate and radiate a discrete spectrum of GWs with frequencies given by

$$\tilde{f} = 2k/l(\tilde{t}), \qquad k \in \mathbb{Z}^+. \tag{2.6}$$

The frequency today is given by $f = \tilde{f}a(\tilde{t})/a_0$. The GW emission power by a loop is independent of its size, which is a remarkable result of the quadrupole formula [124]. For each Fourier mode k, it is given by

$$P_{\rm GW}^{(k)} = \Gamma^{(k)} G\mu^2, \qquad \text{with} \quad \Gamma^{(k)} = \frac{\Gamma k^{-\delta}}{\sum_{p=1}^{\infty} p^{-\delta}}, \tag{2.7}$$

and $\Gamma = 50$ for local [158] and global strings [159]. The index δ depends on whether high Fourier modes are dominated by cusps ($\delta = 4/3$), kinks ($\delta = 5/3$), and kink-kink collisions ($\delta = 2$) [160]. This choice does not impact much the amplitude of the GW spectrum in the deep RD and MD era, but it substantially impacts the slope around the transition between early MD and RD, see section 3.1. In this work, we assume the small-scale structure to be dominated by cusps $\delta = 4/3$. While loops continuously lose energy as they emit either GWs or Goldstone modes, their length l shrinks as

$$l(\tilde{t}) = \alpha t_i - (\Gamma G\mu + \kappa)(\tilde{t} - t_i). \tag{2.8}$$

where $\Gamma G\mu$ and κ are the shrinking rates due to GW and particle emissions, respectively. Local-string loops dominantly decay via GW emission ($\kappa = 0$), while global-string loops dominantly decay into Goldstone modes with $\kappa = \Gamma_{\rm Gold}/2\pi \log(\eta t) \gg \Gamma G\mu$ where $\Gamma_{\rm Gold} \simeq 65$ [161].

2.2 GW spectrum

From right to left, we write in chronological order the different involved processes leading to the final expression for the spectral energy density of GWs from CS, defined as $\Omega_{\rm GW} \equiv \frac{1}{\rho_c}\frac{d\rho_{\rm GW}}{d\ln f}$,

$$\begin{aligned}\Omega_{\rm GW}(f) = \sum_k \frac{1}{\rho_c}\int_{t_{\rm osc}}^{t_0} d\tilde{t} \int_0^1 d\alpha\, \Theta\left[t_i - \frac{l_*}{\alpha}\right] \cdot \Theta[t_i - t_{\rm osc}] \cdot \left[\frac{a(\tilde{t})}{a(t_0)}\right]^4 \cdot P_{\rm GW}^{(k)} \times \\ \times \left[\frac{a(t_i)}{a(\tilde{t})}\right]^3 \cdot \mathcal{P}_{\rm loop}(\alpha) \cdot \frac{dt_i}{df} \cdot \frac{dn_{\rm loop}}{dt_i}.\end{aligned} \tag{2.9}$$

First, loops are formed at a rate $dn_{\rm loop}/dt_i$ (note the chain rule dt_i/df) with a distribution of size $\mathcal{P}_{\rm loop}(\alpha)$. They redshift like a^{-3} before radiating GW with power $P_{\rm GW}^{(k)}$ which subsequently dilute as a^{-4}. We add two Heaviside functions to cut off the GW spectrum above some characteristic frequencies discussed below. Finally, we integrate over all loop sizes α and GW emission times $\tilde{t}$ and sum over all Fourier modes k.

The first Heaviside function $\Theta(t_i - l_*/\alpha)$ eliminates loops smaller than a critical length l_* below which massive particle production is the main decay channel [124, 162]. The second Heaviside function $\Theta(t_i - t_{\rm osc})$ with $t_{\rm osc} = {\rm Max}\,[t_{\rm form}, t_{\rm fric}]$ gets rid of loops which would have formed before the formation of the network, cf. eq. (2.2), or which form in the friction-dominated epoch, cf. eq. (2.3). As shown in [124], these high-frequency cut-offs lie at frequencies higher than the windows of current and future GW interferometers. After this short introduction, we simplifies eq. (2.9) to the handy form,

$$\Omega_{\rm GW}(f) = \sum_k \frac{1}{\rho_c} \cdot \frac{2k}{f} \cdot \frac{(0.1)\,\Gamma^{(k)} G\mu^2}{\alpha(\alpha+\Gamma G\mu+\kappa)} \times \\ \times \int_{t_{\rm osc}}^{t_0} d\tilde{t}\, \frac{C_{\rm eff}(t_i)}{t_i^4} \left[\frac{a(\tilde{t})}{a(t_0)}\right]^5 \left[\frac{a(t_i)}{a(\tilde{t})}\right]^3 \Theta\left(t_i - \frac{l_*}{\alpha}\right) \Theta(t_i - t_{\rm osc}). \tag{2.10}$$

This formula can be used for both local and global strings after applying eqs. (2.6) and (2.8) and choosing an appropriated value of κ. The resulting GW spectra assuming the standard ΛCDM Universe are illustrated by the black dashed lines in figure 1. For loops formed and emitted during radiation-domination epoch, the GW spectrum emitted by local strings is nearly flat with an amplitude of order[2]

$$\Omega^{\rm CS}_{\rm std} h^2 \simeq \Omega_r h^2 \mathcal{G}(\tilde{T}_{\rm M}) \left(\frac{\eta}{M_{\rm pl}}\right), \tag{2.12}$$

where $\Omega_r h^2 \simeq 4.2 \times 10^{-5}$ [163] is the radiation density today and $\tilde{T}_{\rm M}$ is the temperature at time $\tilde{t}_{\rm M}$ of maximum emission defined in eq. (2.16). Deviations from flatness arise due to a change in the number of relativistic degrees of freedom captured in [124]

$$\mathcal{G}(T) \equiv \left(\frac{g_*(T)}{g_*(T_0)}\right)\left(\frac{g_*s(T_0)}{g_{*s}(T)}\right)^{4/3} = 0.39\left(\frac{106.75}{g_*(T)}\right)^{1/3}. \tag{2.13}$$

In comparison, the GW spectrum from global strings is suppressed by $(\eta/M_{\rm pl})^3$ due to the shorter loop lifetime and enhanced by a $\log^3$ factor due to the larger string tension[3]

$$\Omega^{\rm CS}_{\rm std} h^2 \sim \Omega_r h^2 \mathcal{G}(\tilde{T}_{\rm M}) \left(\frac{\eta}{M_{\rm pl}}\right)^3 \log^3\left(\eta \tilde{t}_{\rm M}\right). \tag{2.15}$$

We refer to ref. [124] for a detailed discussion about the differences between GW from local and global strings. The impact of a non-standard cosmological evolution, such as a PBH-dominated universe, is studied in section 4.

2.3 Temperature-frequency relation

The dominant emission in GW arises at the end of the loops lifetime when the loop size in eq. (2.8) is half its initial size $l(\tilde{t}_{\rm M}) = \alpha t_i/2$ [122, 124]

$$\tilde{t}_{\rm M} = \frac{\alpha/2 + \Gamma G\mu + \kappa}{\Gamma G\mu + \kappa} t_i \simeq \begin{cases} \frac{\alpha}{2\Gamma G\mu} t_i & \text{for } \kappa = 0,\ \alpha \gg \Gamma G\mu \quad \text{(local)}, \\ t_i & \text{for } \kappa \gg \alpha \gg \Gamma G\mu \quad \text{(global)}. \end{cases} \tag{2.16}$$

[2] Keeping all the parameters, we get [124]

$$\Omega^{\rm CS}_{\rm std} h^2 \simeq 1.5\pi \Omega_r h^2\, \mathcal{G}\, C^{\rm rad}_{\rm eff} \left(\frac{\alpha G\mu}{\Gamma}\right)^{1/2}, \qquad \text{(local)}. \tag{2.11}$$

[3] The GW spectrum of global strings in radiation-dominated universe reads [124]

$$\Omega^{\rm CS}_{\rm std} h^2 \simeq 9 \Omega_r h^2\, \mathcal{G}(\tilde{T}_{\rm M})\, C^{\rm rad}_{\rm eff} \left(\frac{\Gamma}{\Gamma_{\rm gold}}\right) \left(\frac{\eta}{M_{\rm pl}}\right)^4 \log^3\left(\eta \tilde{t}_{\rm M}\right), \qquad \text{(global)}. \tag{2.14}$$

The global-string loops decay fast after their production, while the local-string loops live much longer. The frequency today f is related to the emitted frequency $\tilde{f}$ by $f = \tilde{f} \times a(\tilde{t})/a_0$. The emitted frequency $\tilde{f}$ is related to the loop length $l(\tilde{t}_M) = \alpha t_i/2$ by eq. (2.6). Assuming RD followed by the standard ΛCDM evolution after loop formation, we obtain the relation between the GW frequency today and the temperature when the loop dominantly sourcing this frequency mode is produced

$$f_\Delta \simeq \begin{cases} (2\times 10^{-3}\ \text{Hz}) \left(\frac{0.1\times 50\times 10^{-11}}{\alpha\times\Gamma G\mu}\right)^{1/2} \left(\frac{T_\Delta}{\text{GeV}}\right) \left[\frac{g_*(T_\Delta)}{g_*(T_0)}\right]^{\frac{1}{4}} & \text{(local strings)}, \\ (4.7\times 10^{-6}\ \text{Hz}) \left(\frac{0.1}{\alpha}\right) \left(\frac{T_\Delta}{\text{GeV}}\right) \left[\frac{g_*(T_\Delta)}{g_*(T_0)}\right]^{\frac{1}{4}} & \text{(global strings)}, \end{cases} \tag{2.17}$$

We have multiplied the numerical-fitted factors[4] of ≈ 0.03 and ≈ 0.2 for local and global strings, respectively, to account for VOS evolution [124].

We now use eq. (2.17) to compute the frequencies beyond which the GW spectrum is cut off due to network formation, friction, and particle production. Those cut-offs are away from the reach of current and planned GW interferometers. This has to be contrasted with the frequency of the turning point caused by the presence of an early matter-domination era — and in particular, a PBH-dominated era — which can lie within the detectable windows.

Formation cut-off. No GW can be produced before the cosmic strings network is formed. Plugging the temperature at which the U(1) symmetry is spontaneously broken in eq. (2.2) into eq. (2.17) leads to the high-frequency cut-off

$$f_{\text{form}} \simeq \begin{cases} 206\ \text{GHz} \left(\frac{0.1\times 50}{\alpha\Gamma}\right)^{\frac{1}{2}} \left[\frac{g_*(T_{\text{form}})}{g_*(T_0)}\right]^{\frac{1}{4}} & \text{for local}, \\ 0.47\ \text{GHz} \left(\frac{T_{\text{form}}}{10^{14}\ \text{GeV}}\right) \left(\frac{0.1}{\alpha}\right) \left[\frac{g_*(T_{\text{form}})}{g_*(T_0)}\right]^{\frac{1}{4}} & \text{for global}, \end{cases} \tag{2.18}$$

where T_0 denotes the temperature of the Universe today. We recall that α is the string size at formation in a unit of the cosmic horizon and Γ is the GW emission efficiency of a string loop.

Friction cut-off. GW emission starts when effects from friction become negligible and cosmic strings start oscillating at relativistic speed. Plugging eq. (2.3) into eq. (2.18), we obtain the high-frequency cut-off due to loop motion being frozen at earlier times

$$f_{\text{fric}} \simeq \begin{cases} \frac{5\times 10^7\ \text{Hz}}{\beta} \left(\frac{0.1\times 50\times G\mu}{\alpha\Gamma\times 10^{-11}}\right)^{\frac{1}{2}} \left[\frac{g_*(T_{\text{fric}})}{g_*(T_0)}\right]^{\frac{1}{4}} \left[\frac{g_*(T_{\text{fric}})}{100}\right]^{\frac{1}{2}} & \text{for local}, \\ \frac{5.6\times 10^3\ \text{Hz}}{\beta} \log(\eta\tilde{t}_M) \left(\frac{\eta}{10^{14}\ \text{GeV}}\right)^2 \left(\frac{0.1}{\alpha}\right) \left[\frac{g_*(T_{\text{fric}})}{g_*(T_0)}\right]^{\frac{1}{4}} & \text{for global}. \end{cases} \tag{2.19}$$

Massive particle production cut-offs. As previously discussed, global strings exhibit suppressed GW emission due to the efficient production of massless Goldstone modes. On the other hand, particles in the gauge sector of local strings are massive, resulting in

[4]Since these factors depend on how fast the string network evolves, the local-string network reaches the scaling regime slower than the global string. The reason is that global strings lose energy more efficiently than local strings.

JHEP08(2023)196

significant suppression of their production rate [164–166]. The emission of massive particles occurs when Fourier modes surpass the mass gap, which happens during cusps or kink-kink collisions. It has been found that the power emitted in massive particles only exceeds the power emitted in GWs for loops smaller than the critical length [124, 162][5]

$$l_{\rm part} = \beta_m \frac{\mu^{-1/2}}{(\Gamma G\mu)^m}, \tag{2.20}$$

where $m = 1$ or 2 for loops kink-dominated [170] or cusp-dominated [171–173], respectively, and $\beta_m \sim \mathcal{O}(1)$. Loops with lengths smaller than $l_{\rm part}$ should be subtracted when computing the SGWB. Plugging eq. (2.20) into eqs. (2.6) and (2.17) gives the frequency cut-offs

$$f_{\rm part} \simeq \begin{cases} (0.5\ \text{GHz})\ \sqrt{\dfrac{1}{\beta_c}}\left(\dfrac{G\mu}{10^{-15}}\right)^{1/4} & \text{for kinks,} \\ (100\ \text{GHz})\ \sqrt{\dfrac{1}{\beta_k}}\left(\dfrac{G\mu}{10^{-15}}\right)^{3/4} & \text{for cusps.} \end{cases} \tag{2.21}$$

2.4 Current constraints on cosmic strings

Local strings. An SGWB might have been detected by pulsar timing arrays NANOGrav [174], EPTA [175], PPTA [176], and IPTA [177]. The signal from NANOGrav can be interpreted as an SGWB from cosmic strings with tension $G\mu \sim 8\times 10^{-11}$ [125, 178]. This interpretation is less favored by other PTAs which prefer a harder spectrum [179, 180]. Analysis of the PPTA data set provides the upper bound $G\mu \leq 5 \times 10^{-10}$ [180].

Other signatures from Nambu-Goto strings result from the static gravitational field around the string. This can induce gravitational lensing and temperature anisotropies in the CMB. The resulting constraint $G\mu \lesssim$ few $\times\, 10^{-7}$, e.g., [181, 182], is however much looser than the one from GW production. However, a recent study has shown that the strong gravitational lensing of the fast radio bursts could probe down to $G\mu \sim 10^{-9}$ with future radio telescopes [183].

Global strings. Global cosmic strings efficiently produce massless Goldstone particles that contribute to the number $N_{\rm eff}$ of effective relativistic degrees of freedom. The precise constraint relies on the abundance of Goldstone particles from strings which is still debatable.[6] We quote the upper bound $\eta \lesssim 3.5 \cdot 10^{15}$ GeV derived in ref. [156] and refer to refs. [159, 190] for slightly tighter bounds.

The absence of B-mode polarization in the CMB provides another constraint on global strings. Assuming instantaneous reheating and only SM degrees of freedom, the upper limit on the inflationary Hubble parameter $H_{\rm inf} \lesssim 3 \times 10^{13}$ GeV [138] translates to the maximum temperature of the universe $T_{\rm max} \lesssim 4 \times 10^{15}$ GeV. For the string network to form, the string scale η must be smaller than the maximum temperature $\eta \lesssim 4 \times 10^{15}$ GeV, up to $\mathcal{O}(1)$ model-dependent parameters.

[5]See [167–169] for different findings.

[6]Recent studies [184–187] propose that the Goldstone energy spectrum from strings is scale-invariant, while other studies [159, 188, 189] suggest a slightly infrared-dominated spectrum, which leads to the production of more Goldstone particles.

JHEP08(2023)196

For $\eta \gtrsim 10^{15}$ GeV, GW from global strings extend to $f \lesssim 10^{-14}$ Hz which could leave signature in CMB polarization experiments, e.g. ref. [138]. Nonetheless, GW in this frequency range is produced after photon decoupling, and the CMB constraint is evaded; see eq. (2.17) or figure 8 of ref. [156].

3 GW signatures from an early matter-dominated era

We consider a period of early matter domination (EMD) inside the usual radiation era. We parametrize the EMD era by two parameters: 1. the temperature $T_{\rm dec}$ of the thermal plasma when the EMD ends, and 2. the duration of the EMD characterized by the number of e-folds $N_{\rm MD}$ of cosmic expansion,

$$\exp(N_{\rm MD}) \equiv \frac{a(T_{\rm dec})}{a(T_{\rm dom})} = \left[\frac{g_*(T_{\rm dom})}{g_*(T_{\rm dec})}\right]^{1/3} \left(\frac{T_{\rm dom}}{T_{\rm dec}}\right)^{4/3}, \tag{3.1}$$

where $T_{\rm dom}$ is the radiation temperature when the EMD era starts. During a matter era, the universe expands faster than during a radiation era, inducing a *double-step* and *single-step* suppression of the GW spectrum from local and global strings, respectively, see figure 1.

In this section, we scrutinize these *step* signals and find three smoking-gun features — shown in figure 2 — which carry direct information about the EMD:

Features	EMD Info.	Expressions
I. Low-frequency (LF) turning point	$T_{\rm dec}$	eq. (2.17)
II. High-frequency (HF) plateau	$N_{\rm MD}$	eq. (3.5)
III. *Knee* (only local strings)	$T_{\rm dec}$, $N_{\rm MD}$	eqs. (3.6)–(3.7).

In the following subsections, we discuss their origins, derive the value of the frequency at their position, and calculate their detectability in future GW observatories. We emphasize that the present paper is the first to introduce the *double-step* feature; see section 3.4 for more details.

3.1 Spectral index

Cosmic-strings GW via a *two-step* process. As mentioned in section 2, the cosmic-string network first produces string loops whose energy density red-shifts as non-relativistic matter, $\rho_{\rm loop} \propto a^{-3}$. Loops dominantly contribute to the GW spectrum at a time $\tilde{t}_M$. It is defined by the time when the string length has shrunk by a factor two $l(\tilde{t}_M) = l(t_i)/2$; see eq. (2.16). The fraction of energy density in GW today from cosmic-string loops — produced at time t_i and emitting GW at time $\tilde{t}_M$ — is

$$\Omega_{\rm GW}^{\rm CS}(f) = \left(\frac{\rho_{\rm GW}}{\rho_{\rm tot}}\right)\bigg|_0 \simeq \frac{\rho_{{\rm loop},i}}{\rho_{{\rm tot},i}} \cdot \left(\frac{H_i}{H_0}\right)^2 \left(\frac{a_i}{a_M}\right)^3 \left(\frac{a_M}{a_0}\right)^4 \propto \left(\frac{H_i}{H_0}\right)^2 \left(\frac{a_i}{a_M}\right)^3 \left(\frac{a_M}{a_0}\right)^4, \tag{3.2}$$

where i, M, and 0 denote the epochs of loop formation, main GW emission, and today, respectively. These three epochs are related through eq. (2.16) and $f \simeq (4k/(\alpha t_i))(a_M/a_0)$,

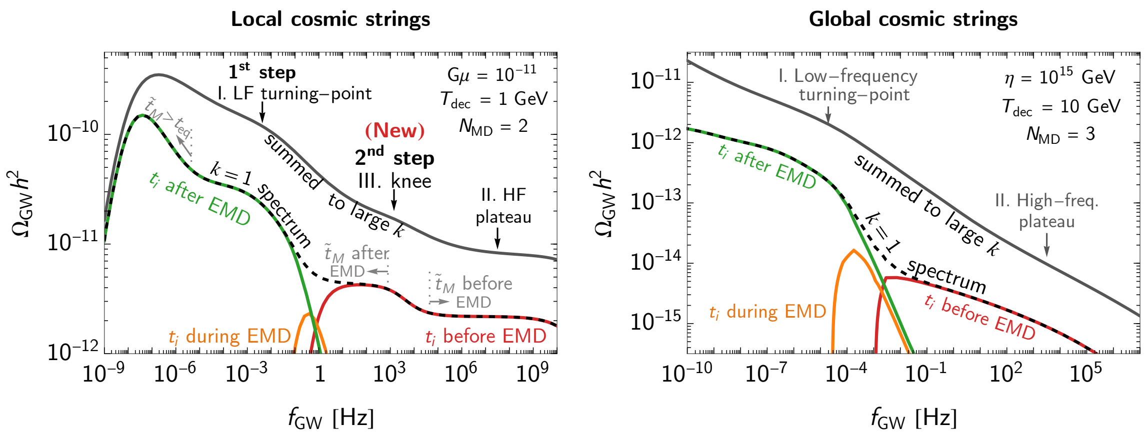

Figure 2. **Left:** three features in the local-string GW spectrum induced by the EMD era. Their origins can be understood, from the ($k = 1$) spectrum, as different loop populations produced at time t_i and emitting GW at time $\tilde{t}_M$ before and/or after the EMD era. The GW spectrum from the local string shows a double-step feature. The steep slope of the 1st step is caused by loops formed during the matter era. The steep slope of the 2nd step results from loops decaying during the matter era. The knee is defined as the local maximum of the second step. **Right:** for global strings, the GW spectrum exhibits a single step due to the loop lifetime being short.

cf. eq. (2.6). In eq. (3.2), we have used that $\rho_{\rm loop,M} \simeq \rho_{\rm GW,M}$ (from energy conservation), $\rho_{\rm loop} \propto a^{-3}$, $\rho_{\rm GW} \propto a^{-4}$, and $\rho_{{\rm loop},i} \propto \rho_{{\rm tot},i}$ (due to the scaling regime). The GW amplitude today in eq. (3.2) is sensitive to the cosmic history around the time t_i of loop production and the time $\tilde{t}_M$ of GW emission. For global strings, the short loop lifetime implies that the two processes are simultaneous, and the GW emission occurs as soon as the loop is formed $\tilde{t}_M \simeq t_i$.

Fundamental Fourier mode only. We assume that the universe evolves as $\rho_{\rm tot} \propto a^{-n}$ and a^{-m} around loop formation at t_i and dominant GW emission at $\tilde{t}_M$ respectively. The first Fourier mode $k = 1$ of the GW spectrum in eq. (2.10) can be expressed as the power-law

$$\Omega_{\rm GW}^{\rm CS} \propto \mathcal{B}(f) f^{\beta}, \tag{3.3}$$

where $\mathcal{B}(f)$ and β have analytical expressions [22] (see also [101, 121, 122, 124, 155, 156]),[7]

	local	global
$\mathcal{B}(f)$	1	$\log^3\left[(5.6\cdot 10^{30})\left(\frac{\eta}{10^{15}\,\rm GeV}\right)\left(\frac{1\,\rm mHz}{f_{\rm dec}}\right)^2\left(\frac{f_{\rm dec}}{f}\right)^{n/(n-2)}\right]$
β	$2\left[\frac{3m+n(1-m)}{n(2-m)}\right]$	$2\left(\frac{n-4}{n-2}\right)$,

where $f_{\rm dec}$ is the GW frequency related via eq. (2.17) to the temperature when the Universe becomes radiation-dominated again. The GW spectrum exhibits different characteristics

[7]In particular, see [101] for a derivation using eq. (3.2).

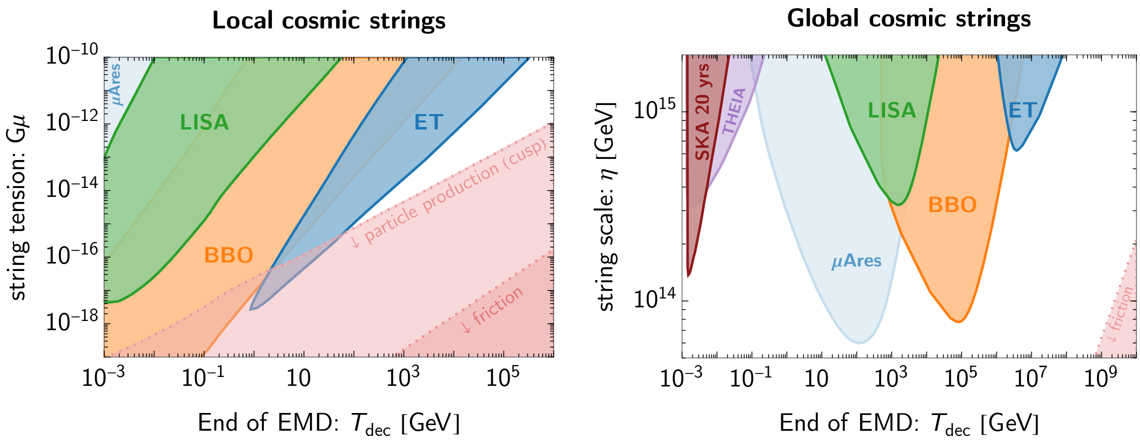

Figure 3. Detectability of the low-frequency turning point, associated with $T_{\rm dec}$ when the EMD era ends; cf. eq. (2.17). The regions correspond to the detection of SNR ≥ 10. The red regions correspond to the cusp and friction cut-offs in eqs. (2.19) and (2.21) that erase the LF turning point.

depending on when the loop formation and emission occur in the history of the universe. For instance, when both events occur during radiation domination with $n = m = 4$, the GW spectrum is flat in frequencies f^0. On the other hand, when a loop forms during matter domination with $m = 3$ and emits during radiation domination with $n = 4$, the resulting spectrum has a tilt of f^{-1}. Finally, when loop formation and GW emission happen during matter domination with $m = n = 3$, the analytical prediction for the spectral tilt is f^{-2}. This result contradicts numerical simulations, as shown in figure 1, where f^{-1} is observed. The reason for this discrepancy is that the assumption of a single time $\tilde{t}_M$ for GW emission is no longer valid in this regime.

Effect from higher Fourier modes. The discussion in the paragraph above only includes the fundamental mode $k = 1$. Effects from higher Fourier modes have been shown in [124, 156, 191] to lead to a departure from f^{-1},

$$\Omega_{\rm GW}^{\rm CS} \propto \begin{cases} f^0, & f \lesssim f_{\rm dec}, \\ f^{\delta-1}, & f_{\rm dec} \lesssim f \lesssim k_{\max} f_{\rm dec}, \\ f^{-1}, & f \gtrsim k_{\max} f_{\rm dec}, \end{cases} \tag{3.4}$$

where $k_{\max}$ is the maximal excited Fourier mode, which can be quite large cf. eq. (A.2) in appendix A, and δ is the spectral tilt of the GW emission power of a string loop, cf. eq. (2.7). In this paper, we assume a cusp-dominated small-scale structure for which $\delta = 4/3$ [160]. We obtain the spectral index $f^{-1/3}$. For long matter era, we indeed observe a spectral slope $-1/3$, see figure 2 and 4. For the short matter era, a more complex spectral shape emerges, with a distinctive *knee*.

3.2 Low-frequency turning point

The low-frequency (LF) turning point separates GWs emitted by loops formed during the radiation era, characterized by a slope f^0, from those formed during the matter era, characterized by a slope f^β with $0 < \beta \leq 1/3$. The frequency $f_{\rm dec}$ of the LF turning point in eq. (2.10) is sensitive to the temperature $T_{\rm dec}$ at which the EMD era ends. Figure 3 shows the parameter space where future GW experiments can detect the LF turning point for both local and global cosmic strings. The detection criterion for this analysis is SNR ≥ 10, obtained by comparing the GW signal with the power-law integrated sensitivity curves defined in appendix D. The red regions in the figure indicate where the particle production and friction cut-offs, given by eqs. (2.19) and (2.21), respectively, lies at higher frequencies than $f_{\rm dec}$.

3.3 High-frequency plateau

The plateau at high-frequency results from GW emitted during the radiation era preceding the EMD era at a temperature $T_{M,\rm HF} > T_{\rm dom}$. $T_{M,\rm HF}$ is the temperature when loop produced at $T_{\rm HF}$ release most of their energy into GW. From eq. (3.2), GW in the HF plateau is suppressed with respect to GW at the LF turning point by

$$\begin{aligned}
\frac{\Omega_{\rm GW}^{\rm HF-plateau}}{\Omega_{\rm GW}^{\rm dec}} &\simeq \left(\frac{H_{\rm HF}}{H_{\rm dec}}\right)^2 \left(\frac{a_{M,\rm HF}}{a_{M,\rm dec}}\right)^4 \left(\frac{a_{\rm HF}}{a_{M,\rm HF}}\right)^3 \left(\frac{a_{M,\rm dec}}{a_{\rm dec}}\right)^3, \\
&\simeq \left(\frac{a_{\rm dom}}{a_{\rm dec}}\right) \left(\frac{a_{\rm dec}}{a_{M,\rm dec}}\right) \left(\frac{a_{M,\rm HF}}{a_{\rm HF}}\right) \left(\frac{\mathcal{G}(T_{\rm HF})}{\mathcal{G}(T_{\rm dom})}\right), \\
&\simeq \exp(-N_{\rm MD}) \left[\frac{\mathcal{G}(T_{\rm dec})\mathcal{G}(T_{M,\rm HF})\mathcal{G}^3(T_{\rm HF})}{\mathcal{G}(T_{M,\rm dec})\mathcal{G}^4(T_{\rm dom})}\right]^{1/4}, \qquad (3.5)
\end{aligned}$$

where the second step uses $\rho_{\rm MD} \propto a^{-3}$ and $\rho_{\rm RD} \propto a^{-4}\mathcal{G}(T)$ with $\mathcal{G}(T)$ in eq. (2.13), and the third step uses $a(t) \propto \mathcal{G}^{1/4}(T)t^{1/2}$ (from Friedmann's equation) and the loop lifetime in eq. (2.16). $T_{M,\rm dec}$ is the temperature when loop produced at $T_{\rm dec}$ release most of their energy into GW. The function $\mathcal{G}(T)$ varies from $\simeq 0.4$ at high temperatures to 1 at low temperatures. The last bracket reduces to $\mathcal{O}(1)$ and 1 for local and global strings respectively. The suppression of the HF plateau encoded in eq. (3.5) is visible in figure 1. In appendix C.1, we also show the cosmic-string GW spectrum when the number of degrees of freedom g_* and g_{*s} are fixed, i.e. taking $\mathcal{G}(T) \equiv 1$. For the global string, the HF plateau f^0 has a distinct HF turning point at $f = f_{\rm dec}$ below which the slope turns to $f^{1/3}$. In appendix B, we provide an analytic formula for the HF turning point of global strings and argue that it is difficult to detect, e.g., see figure 11. For local string, the spectral slope below $f < f_{\rm dec}$ is not exactly $-1/3$ due to the '*knee*' feature, which we now discuss below.

3.4 The knee feature

In the case of local strings, the GW spectrum has an additional feature due to loops living longer than the duration of the EMD. In figure 2, we show for the first time that the EMD imprints not only one but two steps in the GW spectrum. They originate from

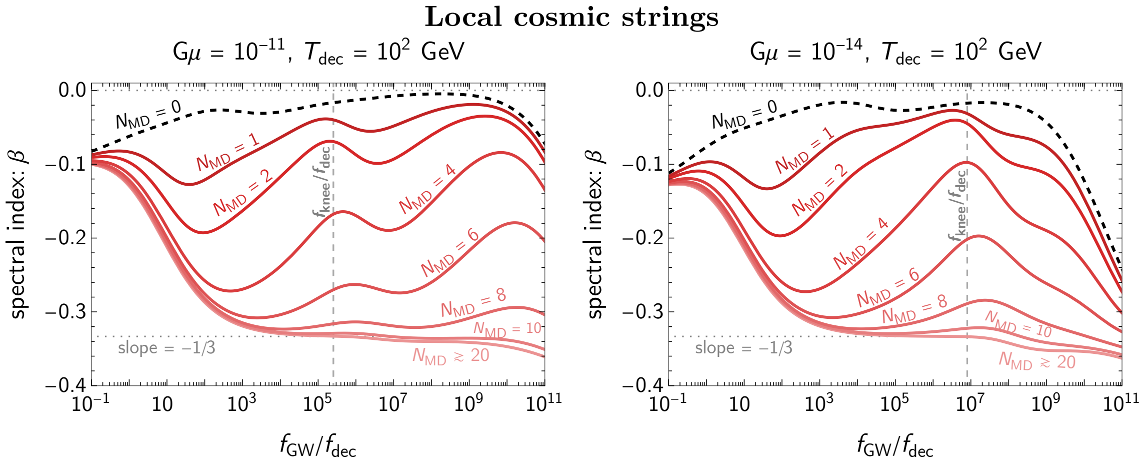

Figure 4. Numerical result of the spectral slope (i.e., $\beta \equiv d \log \Omega_{\rm GW}/d \log f$) of the local-string GW experiencing different duration $N_{\rm MD}$ of the EMD era. The vertical dashed lines show the position of the *knee* feature, specified by eq. (3.7). Only for $N_{\rm MD} \gtrsim 10$ (cf. appendix C.2), the *knee* feature submerges below the $-1/3$-slope tail from the LF turning point.

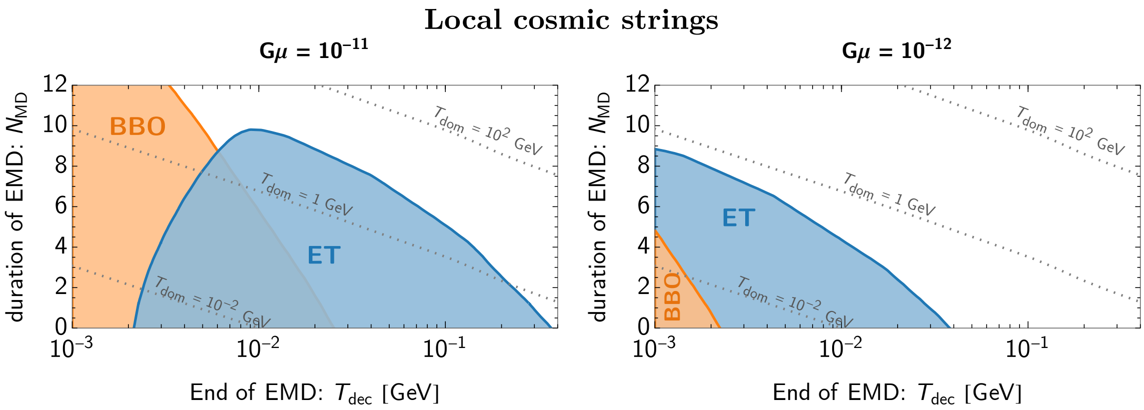

Figure 5. Detectability of the *knee* feature at future GW observatories. Its observation provides information about the energy scale and duration of the EMD. We cut the parameter space to $N_{\rm MD} < 12$ because the *knee* visibility is lost for larger $N_{\rm MD}$; see appendix C.2 for more details.

the production of GWs occurring in two steps: first, loops are formed at a time t_i, and second, they decay at a later time $\tilde{t}_M$. The first step suppression in the GW spectrum is attributed to the formation of loops during the EMD, while the higher-frequency step suppression results from the decay of loops during the EMD. The intermediate region of the GW spectrum is sourced by string loops that formed prior to the onset of the EMD era and emitted most of their energy into GWs after the EMD era ended. Figure 4 shows the numerical results of the spectral slopes for different $G\mu$ and EMD durations. We call the *knee* the local maximum of the second step, between the LF turning point and the HF plateau; see the vertical dashed line. The *knee* feature can also be seen clearly in figures 1 and 2. Such features do not show up in the GW spectrum from global strings because the short lifetime of loops merges the two steps into one.

JHEP08(2023)196

Although the *knee* feature is the smoking-gun signature of the EMD era, the same underlying physics can also leave an imprint on the local-string GW spectrum, assuming the standard ΛCDM history [158], shown in figure 1. The spectral peak — located around $f_{\rm GW} \simeq 150$ nHz $(50 \cdot 10^{-11})/(\Gamma G\mu)$ [124] — has its UV slope from loops with $t_i < t_{\rm eq} < \tilde{t}_M$ and its IR cut-off due to the matter-Λ transition. Nonetheless, no knee feature is present for the standard cosmological history due to the lack of a double-step spectrum, unlike the EMD case.

We now analytically estimate the position of the *knee* feature and calculate its detectability by future GW observatories. The spectral slope reaches its maximum — the tip of the *knee* — when the time $\tilde{t}_M$ of dominant GW emission occurs at the very end of the EMD $\tilde{t}_M = t_{\rm dec}$; see figures 2 and 5. Using eq. (3.2) with $a_{M,\rm knee} = a_{\rm dec}$, we obtain an analytic estimation for the GW amplitude at the *knee*,

$$
\begin{aligned}
\frac{\Omega_{\rm GW}^{\rm knee}}{\Omega_{\rm GW}^{\rm dec}} &\simeq \left(\frac{H_{\rm knee}}{H_{\rm dec}}\right)^2 \left(\frac{a_{\rm dec}}{a_{M,\rm dec}}\right)^4 \left(\frac{a_{\rm knee}}{a_{\rm dec}}\right)^3 \left(\frac{a_{M,\rm dec}}{a_{\rm dec}}\right)^3, \\
&\simeq \left(\frac{a_{\rm dom}}{a_{\rm knee}}\right) \left(\frac{a_{\rm dec}}{a_{M,\rm dec}}\right) \left(\frac{\mathcal{G}(T_{\rm knee})}{\mathcal{G}(T_{\rm dom})}\right), \\
&\simeq \exp\left(-3N_{\rm MD}/4\right) \left[\frac{\mathcal{G}(T_{\rm dec})\mathcal{G}^3(T_{\rm knee})}{\mathcal{G}(T_{M,\rm dec})\mathcal{G}^3(T_{\rm dom})}\right]^{1/4},
\end{aligned}
\tag{3.6}
$$

where the second step uses $\rho_{\rm MD} \propto a^{-3}$ and $\rho_{\rm RD} \propto a^{-4}\mathcal{G}(T)$ with $\mathcal{G}(T)$ in eq. (2.13), and the third step uses $a_{\rm RD}(t) \propto \mathcal{G}^{1/4}(T)t^{1/2}$, $a_{\rm MD}(t) \propto t^{2/3}$, and the loop lifetime in eq. (2.16). Applying eqs. (2.6) and (2.16), we arrive at the *knee* frequency,

$$
\begin{aligned}
f_{\rm knee} &\simeq f_{\rm dec}\left(\frac{t_{\rm dec}}{t_{\rm knee}}\right)\left(\frac{a_{\rm dec}}{a_{M,\rm dec}}\right) \simeq f_{\rm dec}\left(\frac{\alpha}{2\Gamma G\mu}\right)^{1/2}\left[\frac{\mathcal{G}(T_{\rm dec})}{\mathcal{G}(T_{M,\rm dec})}\right]^{1/4}, \\
&\simeq 607\,\text{Hz}\left(\frac{50\cdot 10^{-11}}{\Gamma G\mu}\right)\left(\frac{T_{\rm dec}}{\rm GeV}\right)\left[\frac{g_*^2(T_{\rm dec})}{g_*(T_0)g_*(T_{M,\rm dec})}\right]^{\frac{1}{4}}\left[\frac{g_{*s}(T_{M,\rm dec})}{g_{*s}(T_{\rm dec})}\right]^{\frac{1}{3}}
\end{aligned}
\tag{3.7}
$$

where we have used $f_{\rm dec}(T_{\rm dec})$ in eq. (2.17) multiplied by a numerical factor of 33.5)[8] We can see that eq. (3.7) describes well the numerical results in figure 1. In appendix C.1, we show GW spectrum at fix g_* and g_{*s} in order to make effects from the *knee* more visible.

The *knee* feature described by eqs. (3.6) and (3.7) is sensitive to both the duration $N_{\rm MD}$ of the EMD era and its end temperature $T_{\rm dec}$, unlike the low-frequency turning point feature which only depends on the latter. By detecting the *knee* feature, future GW observatories could reconstruct the full EMD era, as shown in figure 5. Even if the *knee* feature lies outside the detectability region, figure 4 indicates that observing a portion of the GW spectrum at frequencies $f > f_{\rm dec}$ would enable determination of the EMD duration

[8]In eq. (2.17), $f_{\rm dec}(T_{\rm dec})$ has already taken into account of the network (VOS) evolution and the smoothening effect from the high Fourier modes which shift the apparent LF turning point lower than the one expected from the analytic estimate from the $k = 1$ spectrum by a factor of 1/33.5; see eq. 28 of ref. [124]. However, our estimation of the knee frequency in eq. (3.7) is based on the $k = 1$ spectrum; hence we will use the LF turning point of the $k = 1$ spectrum.

JHEP08(2023)196

$N_{\rm MD}$. While an analytical expression for the spectral index in figure 4 is challenging to derive due to the effects of higher Fourier modes and GW emission beyond the dominant epoch $\tilde{t}_M$, it remains a topic for future studies.

The presence of a second step in the GW spectrum already appeared in previous numerical calculations, e.g., figure 12 of ref. [124] and figure 9 of ref. [22],[9] but its origin and detectability are studied for the first time in the present paper. This knee feature can potentially serve as a distinguishing characteristic of the EMD signature from the effects of particle production cutoffs [162], which also have a $f^{-1/3}$ slope or supercooling phase transition effects [38] which has peak plus a plateau feature in the GW spectrum. A short intermediate inflation [22, 193, 194] could also lead to similar behaviors, we leave its study for future work.

4 Primordial black holes domination era

After they form in the early Universe, PBHs may be abundant enough to dominate the total energy density before they evaporate through Hawking radiation. Because their mass is relatively constant before Hawking evaporation becomes sizeable, they behave like a component of cold matter in the early Universe. In this section, we explore the possibility that the early matter domination era studied in the previous section, and its effect on the GW spectrum emitted by cosmic strings, are due to the existence of such PBHs.

4.1 PBH formation

PBHs form as a consequence of density fluctuations present in the early universe. When the density in a region exceeds a certain threshold, the gravitational forces become strong enough to overcome the Hubble expansion and pressure [45], leading to gravitational collapse and the formation of a black hole. These fluctuations can arise from various mechanisms, e.g. [46–50, 52–56, 61–63, 65–74, 76, 77, 80–87]. Some scenarios produce PBH distributions that peak at a particular mass, while others result in extended distributions related to the Fourier spectrum of the primordial fluctuations and to the equation of state of the Universe at the time they collapsed [26, 45, 195–198]. Our study avoids making assumptions about the specific mechanism of overdensity formation and simplifies the analysis by considering a nearly-monochromatic density distribution.

$$\frac{dn_{\rm PBH}}{dM_{\rm PBH}} \propto \delta(M - M_{\rm PBH})\,. \tag{4.1}$$

We introduce the parameter γ, which represents the fraction of mass within the Hubble horizon that collapses into a PBH. We can then establish a relationship between the mass $M_{\rm PBH}$ of the PBH and the temperature T_f at which it forms

$$M_{\rm PBH} = \gamma\rho\frac{4\pi}{3}\left(\frac{1}{H(T_f)}\right)^3 \simeq 10^9\ {\rm g}\ \left(\frac{\gamma}{0.2}\right)\left(\frac{100}{g_*(T_f)}\right)^{1/2}\left(\frac{1.4\times10^{11}\ {\rm GeV}}{T_f}\right)^2, \tag{4.2}$$

[9]Non-trivial spectral tilts can also arise in the presence of multiple epochs of EMD [192].

where $g_*(T_f)$ is the number of relativistic degrees of freedom in the plasma at temperature T_f. For PBH collapse occurring from super-horizon fluctuations entering the horizon during RD, we have $\gamma \simeq c_s^3 \simeq 0.2$ where $c_s = 1/\sqrt{3}$ is the speed of sound in a relativistic plasma. The energy fraction of PBHs at formation is defined as

$$\beta(M_{\rm PBH}) \equiv \frac{\rho_{\rm PBH}(T_f)}{\rho_{\rm tot}(T_f)}, \tag{4.3}$$

where $\rho_{\rm tot}(T_f)$ denotes the total energy density in the Universe when the temperature of the SM plasma equals T_f.

4.2 PBH evaporation

The presence of a Schwarzschild horizon implies that PBHs emit a distribution of particles that can be well approximated by a thermal distribution with temperature [88, 89]

$$T_{\rm PBH} = \frac{1}{8\pi G M_{\rm PBH}} \simeq 1.06 \text{ GeV} \left(\frac{10^{13}\text{ g}}{M_{\rm PBH}}\right). \tag{4.4}$$

The corresponding production rate for particle j is

$$\frac{dN_j}{dt dE} = \frac{g_j}{2\pi} \frac{\Gamma_j(E,\, M_{\rm PBH})}{e^{E/T_{\rm PBH}} - (-1)^{s_j}}, \tag{4.5}$$

where g_j is the number of internal degrees of freedom, s_j is its spin, and $\Gamma_j(E,\, M_{\rm PBH})$ is the greybody factor [199, 200]. As a result of Hawking evaporation, the PBH mass decreases at a rate

$$\frac{dM_{\rm PBH}}{dt} = -\sum_j \int_0^\infty dE\, E \frac{dN_j}{dt dE} = -\varepsilon(M_{\rm PBH}) \frac{M_{\rm pl}^4}{M_{\rm PBH}^2}, \tag{4.6}$$

where $M_{\rm pl} \simeq 2.44 \times 10^{18}$ GeV and the function ε is a function that encodes the details of the Hawking emission which depends on the particle physics spectrum considered and the Hawking temperature of the black hole (for a thorough description including the PBH spin, see refs. [201, 202]). In this study, we assume the emitted particles to belong to the SM only,,[10] and since we focus on PBHs with masses $M_{\rm PBH} \lesssim 10^9$ g corresponding to Hawking temperatures $T_{\rm PBH} \gtrsim 10^4$ GeV, all the SM degrees of freedom can be assumed to be relativistic, giving the constant evaporation rate $\varepsilon \simeq 4.4 \times 10^{-3}$.

Upon integrating eq. (4.6) over time, one straightforwardly obtains the lifetime of a PBH with mass $M_{\rm PBH}$ at formation:

$$\tau(M_{\rm PBH}) = \frac{1}{3\varepsilon} \frac{M_{\rm PBH}^3}{M_{\rm pl}^4} \simeq 0.41 \text{ s} \left(\frac{M_{\rm PBH}}{10^9\text{ g}}\right)^3. \tag{4.7}$$

[10] In the case of global strings, the massless scalar boson should, in principle, be added to the discussion. However, it would only affect the results regarding the evaporation temperature by $\mathcal{O}(1\%)$, and can thus be safely ignored here.

JHEP08(2023)196

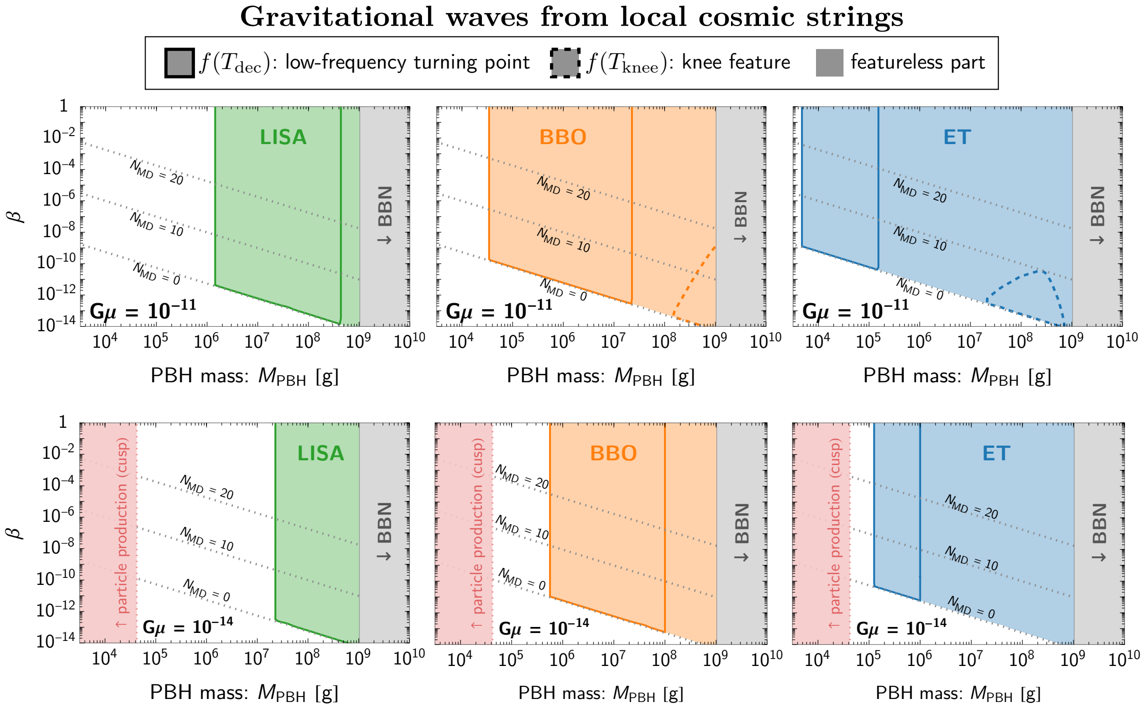

Figure 6. Detectability of the double-step signature from the PBH domination. The regions bounded by the solid and dashed lines correspond to a detectable LF turning point and the knee feature. The unbounded colored region is where the "featureless" part is detectable (information about the duration of PBH domination can be retrieved by measuring the spectral slope, shown in figure 4).

4.3 PBH-dominated era

PBHs smaller than 10^{15} g (150 times the Great Pyramid of Giza) are supposed to have already evaporated by now due to Hawking radiation. PBHs smaller than 10^9 g (one-tenth of the Eiffel tower) have even evaporated before the onset of BBN, leaving not many observables left to probe their existence. However, if their energy fraction β at formation introduced in eq. (4.3) is sufficiently large, PBHs may end up dominating the energy density of the Universe before they evaporate, hence leading to an EMD era. Using that PBHs redshift like matter, we obtain that PBHs domination starts when the temperature of the SM plasma drops below

$$T_{\rm dom} = T_f \beta = 14\,{\rm GeV} \left(\frac{\beta}{10^{-10}}\right)\left(\frac{100}{g_*(T_{\rm f})}\right)^{1/4}\left(\frac{\gamma}{0.2}\right)^{1/2}\left(\frac{10^9\ {\rm g}}{M_{\rm PBH}}\right)^{1/2}, \tag{4.8}$$

where we have used eq. (4.2). After they dominate the total energy density, PBHs reheat the Universe when they evaporate. The reheating temperature $T_{\rm dec}$ immediately after evaporation is the temperature of a radiation-dominated universe whose age is equal to the PBH lifetime in eq. (4.7):

$$T_{\rm dec} \simeq \frac{2.4\ {\rm MeV}}{g_*^{1/4}} \left(\frac{10^9\ {\rm g}}{M_{\rm PBH}}\right)^{3/2}. \tag{4.9}$$

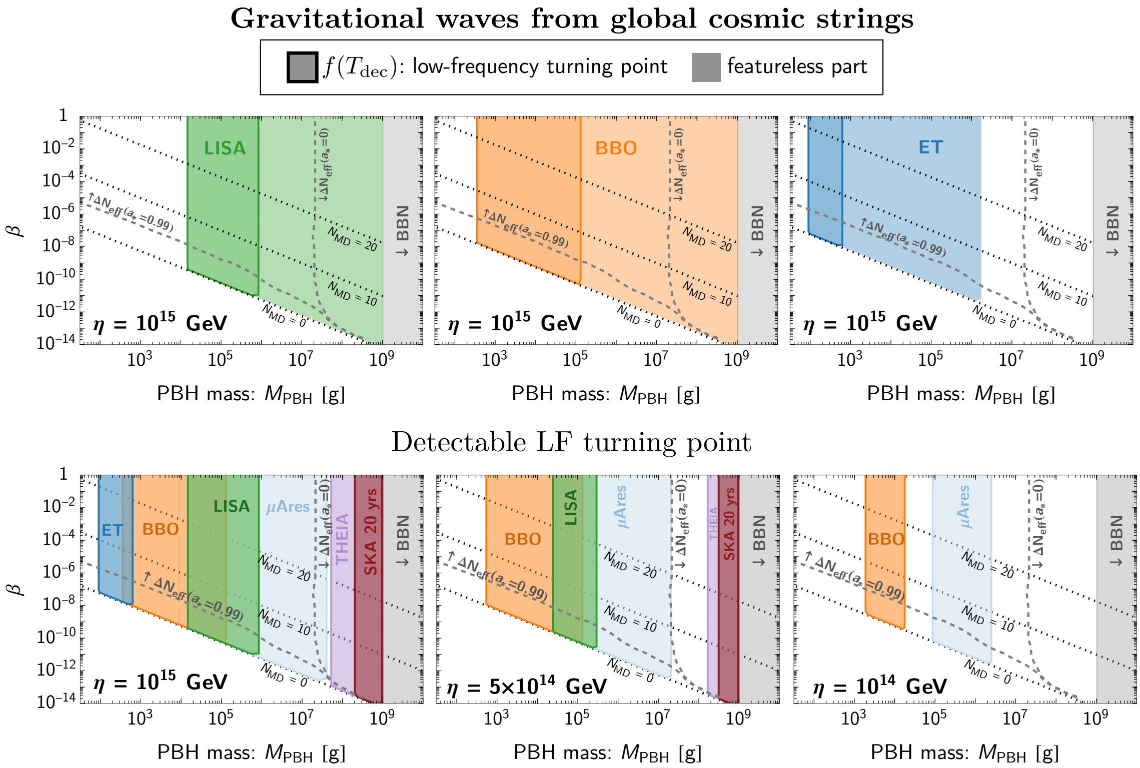

Figure 7. Top panel: detectability of the single-step feature from PBH domination: LF turning point (bounded by solid line) and the featureless part (unbounded). Bottom panel: detectable LF turning point associated with the end of PBH domination in the GW background from global cosmic strings. This is the solely detectable signature on the global-string GW spectrum as the HF turning point locates at the ultra-high frequency and the spectral index is always $-1/3$. Dash lines indicate the $\Delta N_{\rm eff}$ possibly observable by CMB-HD due to the massless goldstone of the global-string U(1) symmetry produced by the evaporation PBH of spin parameter a_*.

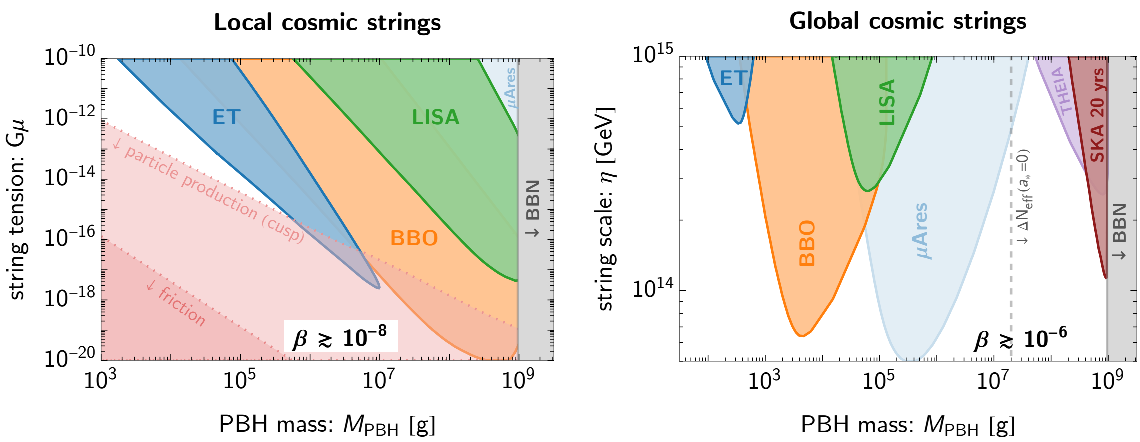

Figure 8. Detectability of the LF turning point due to the PBH domination with varying $G\mu$ (local) and η (global). For global strings, if PBHs have a spin parameter $a_\star = 0.99$, almost the whole parameter space may be probed by CMB-HD; see the previous figure.

JHEP08(2023)196

The condition $T_{\rm dom} > T_{\rm dec}$ needed to have an early period of PBH domination is equivalent to demanding the energy fraction β to be larger than the critical value

$$\beta \ > \ \beta_c \equiv \frac{T_{\rm dec}}{T_f} \simeq 5.5 \times 10^{-15} \left(\frac{0.2}{\gamma}\right)^{1/2} \left(\frac{g_{*,s}(T_f)}{g_*(T_{\rm dec})}\right)^{1/4} \left(\frac{10^9 \text{ g}}{M_{\rm PBH}}\right). \tag{4.10}$$

The total number of e-folds of the corresponding early matter-domination era starting at temperature $T_{\rm dom}$ and ending at temperature $T_{\rm dec}$ can then be simply obtained as

$$N_{\rm MD} = 10 + \log\left[\left(\frac{\gamma}{0.2}\right)^{1/2} \left(\frac{g_{*,s}(T_{\rm dec})}{g_*(T_f)}\right)^{1/4} \left(\frac{M_{\rm PBH}}{10^9 \text{ g}}\right) \left(\frac{\beta(t_f)}{1.2\times 10^{-10}}\right)\right]. \tag{4.11}$$

As discussed in section 3, an early matter-domination era would induce a change of slope in the GW spectrum emitted from a pre-existing cosmic string network. In figure 6, 7, and 8, we show the detection prospects of the imprint of a period of PBH domination by future interferometers.

We consider the PBH-dominated era to be detectable if it leads to a suppression of the GW spectrum larger than 10% as compared to standard cosmology. Using eq. (3.6), one can translate this condition into a threshold on the number of e-folds of PBH domination to be $N_{\rm MD} > 0.14$ or $T_{\rm dom}/T_{\rm dec} \gtrsim 1.11$.

As shown in figure 6, measuring GWs emitted by local-strings with $G\mu = 10^{-11}$ can allow probing the existence of PBHs with masses in the range $[10^6, 10^9]$ g at LISA and $[5\times 10^3, 10^9]$ g at ET. The LF turning-point signature (solid lines) in each detector probes the PBH mass towards the small mass range, while the knee feature (dashed lines) is associated with a larger PBH mass. Interestingly, joint efforts between the different collaborations could allow us to accurately pin down the PBH parameters, e.g., for $G\mu \simeq 10^{-11}$, a PBH of mass $\mathcal{O}(10^8)$ g, and $\beta \sim 10^{-10}$, LISA could observe the LF turning point while ET observes the knee. In the unbounded colored region labeled "featureless part", we show the detectability of the GW spectrum outside the LF turning point and the knee. As shown in figure 4, the non-trivial spectral slope in those regions also carries information about the duration of the PBH domination era.

The ability to probe the PBH parameter space with global-string GWs is shown in figure 7. The top panel provides the observational bounds on the LF turning point and the *featureless* part, while the bottom panel gives more details on the former. From the top panel of figure 7, PBHs with masses $[10^4, 10^9]$ g and $[10^2, 10^6]$ g can be probed by LISA and ET, respectively, with global strings of $\eta = 10^{15}$ GeV. Instead, the bottom panel shows other GW observatories sensitive to LF turning points at frequencies lower than LISA. In contrast to GWs emitted by local strings, whose frequency corresponding to the BBN scale is 10^{-6} Hz, the GWs emitted by global strings can have a LF turning point at smaller frequencies; see eq. (2.17). In this figure, we also show for comparison bounds on PBHs that could be set in the future by CMB-HD, using the fact that massless goldstone bosons may be produced copiously from the evaporation of PBHs and contribute to $\Delta N_{\rm eff}$. As one can see from the figure, in the case of rotating PBHs with spin parameter $a_\star = 0.99$, GW searches and CMB observations may observe complementary smoking-gun signatures

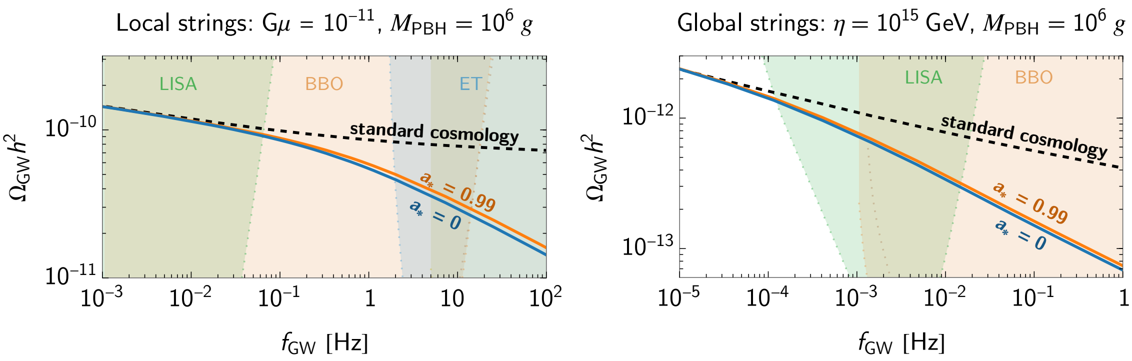

Figure 9. Cosmic-string GW spectra experiencing PBH domination era with the monochromatic PBH mass spectrum $M_{\rm PBH} = 10^6\,$g and $\beta = 10^{-4}$. We vary the PBH spin parameter a_* which affects slightly the lifetime of PBH: $T_{\rm dec} \simeq T_{\rm dec,s}\mathcal{F}^{-1/2}(a_*, M_{\rm PBH})$ for the end of Schwarzschild PBH domination $T_{\rm dec,s}$ and the function $\mathcal{F}$ is taken from ref. [229].

of the existence of a PBH-dominated era, whereas, for Schwarzschild PBHs, GW searches reveal to be much more competitive at low PBH masses.

Figure 8 shows the string-scale ($G\mu$ and η) dependence of the detectability of PBH parameters for large values of β, above which all the shown parameter spaces are guaranteed to have $N_{\rm MD} > 0$; see figures 6 and 7. Note that one loses sensitivity relatively fast in the case of global strings for a decreasing η, as $\Omega_{\rm GW} \propto \eta^4$. Local-string GWs depend on $(G\mu)^{1/2}$. Therefore, even for local strings with a scale as small as $G\mu \sim 10^{-18}$, PBHs can be searched for efficiently by future experiments. Nonetheless, the particle production cutoff could erode the signature from EMD; see eq. (2.21).

4.4 Effects from PBH spins

In the early Universe, PBHs may have acquired angular momentum from merging events [203], matter accretion [204], evaporation [205], primordial inhomogeneities [204], collapse during matter domination [196, 206], or specific mechanisms of PBH formation, such as scalar fragmentation [207, 208], collapse of domain walls [209] or cosmic strings [86, 87]. In that case, the PBHs can be characterized, on top of their mass, by the spin parameter $a_\star = JM_{\rm pl}^2/M_{\rm PBH}^2$ where J is the angular momentum of the black hole. The PBH spin impacts a variety of particle-physics phenomena: e.g., the production of dark matter through evaporation [201, 210–226], the amount of dark radiation produced through evaporation that could contribute to $\Delta N_{\rm eff}$ in future CMB measurements [203, 211, 212, 222, 227, 227–229], or even the spectrum of GW induced at second order in perturbation theory [229]. In this section, we explore the effect of the PBH spin on the PBH domination era and its signature in the cosmic-string GW spectrum.

The spin of PBHs accelerates the dynamics of Hawking evaporation and shortens their lifetime $\Delta t_{\rm PBH}^{\rm Kerr}$ from the expectation $\Delta t_{\rm PBH}^{\rm Sch}$ assuming the Schwarzschild PBH,

$$\Delta t_{\rm PBH}^{\rm Kerr}/\Delta t_{\rm PBH}^{\rm Sch} = \mathcal{F}(a_\star, M_{\rm PBH}), \tag{4.12}$$

where $\mathcal{F}(a_\star, M_{\rm PBH})$ is a numerical function which range from $\mathcal{O}(0.4)$ for $a_\star \simeq 0.999$ to 1 for $a_\star = 0$ and taken from table 1 of ref. [229]. While the start of PBH domination remains unchanged by spin (fixed by the energy fraction at formation β, γ, $M_{\rm PBH}$), the spinning PBHs evaporate at a temperature higher than the Schwarzschild ones, using $\Delta t_{\rm PBH} = H_{\rm PBH}^{-1}$,

$$T_{\rm evap}^{\rm Kerr}/T_{\rm evap}^{\rm Sch} = \mathcal{F}^{-1/2}(a_\star, M_{\rm PBH}) \left[g_*(T_{\rm evap}^{\rm Sch})/g_*(T_{\rm evap}^{\rm Kerr})\right]^{1/4}. \tag{4.13}$$

The evaporation temperature of maximally-spinning PBHs ($a_\star = 0.999 \to \mathcal{F} \simeq 0.4$) is ~ 1.6 times higher than for static PBH, assuming for simplicity $g_{*s}(T_{\rm evap}^{\rm Kerr}) = g_{*s}(T_{\rm evap}^{\rm Sch})$. Concerning the signature in cosmic-string GW, eq. (2.17), the turning point in the case of the maximally-spinning PBHs sits at a frequency ~ 1.6 times higher than in the Schwarzschild case. In figure 9, our results show that effects from spin turn out to be relatively minor. Furthermore, effects from the spin are degenerate with the PBH mass, and they are equivalent to decrease $M_{\rm PBH}$ by a factor 1.4, see eq. (4.9).

5 Conclusion

The cosmological evolution of the universe below a temperature of 5 MeV is well-established and supported by numerous observational probes, including the nuclear abundances predicted by the Big Bang Nucleosynthesis (BBN) epoch, Cosmic Microwave Background (CMB), large-scale structure measurements and supernovae observations. This evolution is characterized by successive epochs of radiation domination, matter domination, and dark energy domination. However, to explore the conditions prevailing in the pre-BBN universe with temperatures above 5 MeV, gravitational waves (GW) are one of the limited observables available. Cosmic strings are one candidate for such sources. They are expected in any high-scale theories of particle physics involving local or global U(1) symmetry breaking ranging from neutrino mass generation, leptogenesis, dark matter, flavor, or Grand Unified Theories in Beyond the Standard Model contexts [145]. An important particularity of cosmic strings is their scaling behavior. Their energy density scales with the scale factor precisely as the dominant energy density of the universe, i.e., a^{-4} during radiation and a^{-3} during matter. Consequently, the spectral slope of the GW energy density is sensitive to the equation of states of the universe at early times.

This study builds upon the research direction "GW archaeology with cosmic strings", initiated in refs. [16, 121, 122, 124, 125]. The objective is to use GW produced by cosmic strings to infer the energy content of the pre-BBN universe. The present work focuses on the GW signatures of an early matter-dominated era. The previous studies assumed that the spectral slope of the GW spectrum emitted by local cosmic strings was independent of the duration $N_{\rm MD}$ of the matter era. An important result of the present work is to reveal the contrary. Figures 1 and 4 show that any measurement of the spectral slope would give information on the duration of the matter era. Until now, only the temperature at the end of the matter era was believed to be measurable. The present study shows that measuring the temperature at which the matter era starts is also possible. As illustrated in figure 2,

JHEP08(2023)196

the impact of the matter era leads to two-step features in the GW spectrum from local strings instead of one, as previously thought. This feature arises due to a GW emission occurring in two steps: first, a string loop is formed at time t_i, and second, the loop converts its energy into GW at the end of its lifetime at $\tilde{t}_M \gg t_i$. The first step in the GW spectrum is due to the impact of the matter era on the scale factor $a(t_i)$, while the second step is due to the impact of the matter era on the scale factor $a(\tilde{t}_M)$. We analytically compute the position of the second step, which we call the *knee*, see eqs. (3.6)–(3.7).

Assuming the standard cosmological history, the cosmic strings with[11] a tension $G\mu \lesssim 10^{-11}$ (local) and an energy scale $\eta \lesssim 10^{15}$ GeV (global) would be observed by LISA, ET, and other future-planned experiments. Our analysis provides a way to extract information about the EMD era, by probing any deviation from the standard-cosmology prediction. As a potential example, we show that the existence of PBHs — if they dominate the energy density of the early universe — can be constrained by LISA and ET for PBH masses between $[10^6, 10^9]$ g and $[5 \times 10^3, 10^9]$ g, respectively, for the local strings with $G\mu = 10^{-11}$. Similarly in the case of global strings, LISA and ET can probe PBH masses between $[10^4, 10^9]$ g and $[10^2, 10^6]$ g, respectively, if the symmetry breaking scale is at $\eta = 10^{15}$ GeV. The detectability and the ability to constrain PBHs become weaker as $G\mu$ and η decrease because the amplitude of the SGWB is smaller, as shown in figure 8. Finally, we considered in section 4.4 the possibility that PBHs are Kerr black holes and therefore evaporate at a slightly earlier time than Schwarzschild black holes.

Current studies [229, 232–239] have demonstrated that scalar-induced GW resulting from adiabatic and isocurvature perturbations can produce distinctive resonant peaks and double-peaks, which can be used to probe the formation and decay time of PBHs in the early universe. These present additional opportunities to test scenarios such as PBH domination and evaporation. The spectral shapes of those GW differ from those found in the context of GW emitted by cosmic strings studied in this work.

Recent pulsar-timing-array data has revealed a common red-noise signal, which may be interpreted as a stochastic GW background in the frequency range $10^{-9}\,\text{Hz} \lesssim f \lesssim 10^{-7}\,\text{Hz}$ [174–177, 230, 240–244]. This signal could potentially be attributed to a cosmic-string network with a tension parameter of $G\mu \in [10^{-11}, 10^{-10}]$ [125, 178, 230]. The early matter era, such as the one induced by PBHs domination, cannot distort the GW spectrum at these low frequencies, as it would require modifying the equation of state of the universe after BBN, which is at odd with concordance cosmology. However, if the signal in the pulsar-timing-array data is caused by cosmic strings, then the high-frequency part of the SGWB spectrum will be detected by future gravitational-wave experiments. Observing this high-frequency component would allow for constraining the presence of any early matter-dominated era occurring below $T \lesssim 10^5$ GeV and for probing the presence of PBHs population down to 10^4 g.

There are some worth-mentioning caveats in our analysis. First, we rely on the detection criterion that requires SNR $= 10$ by comparing our signal to the power-law integrated sensitivity curves. However, this criterion might not be enough when we confront real

[11] Bounded from above by the pulsar-timing-array observations [230, 231].

data. Because the detection claim of a SGWB requires a signal reconstruction over other detectors' noises at an acceptable confidence level, as shown for LISA in [245, 246]. For a spectrum with several features like the *knee*, the detectable signal might have to lie above the detectors' noise level in order to read the SGWB spectrum accurately and to extract precise information about the EMD era. Moreover, the optimal SNR depends on the knowledge about the noises, and one would have to perform a global fit [247] on the combined noises and the SGWB signal. The second caveat is that our work assumes cosmic strings and PBHs do not interact during the PBH-dominated era. However, PBHs can affect the cosmic string network through mechanisms such as chopping off long strings, modifying the network-scaling behavior, suppressing loop production, or leading to necklace-like or net-like structures [248–250]. These processes could result in additional GW contributions [251] beyond our conservative estimates. We leave the study of the string-PBH network for future work.

If the features found in this paper are observed in the GW spectrum from cosmic strings, additional observations will be needed to distinguish between a PBH-dominated era and other forms of early matter domination. It is worth noting that PBHs generate other signals that could be explored in the future. In figure 7, we show possibilities for detecting a non-zero component of dark radiation. Other indicators of the presence of evaporating PBHs in the early universe, such as second-order GWs, dark matter searches, baryogenesis, and structure formation, provide various ways to independently verify the existence of an early PBH-domination era (see e.g. ref. [202] for a recent review). Such detection channels would not only provide valuable independent confirmations of our results but also offer a unique opportunity for synergies between GW searches and CMB, large-scale structure, or even dark-matter search experiments.

The detection of GW has opened up a new avenue for studying the early universe, which is complementary to other methods. Our analysis shows that cosmic strings can serve as excellent standard candles for probing the pre-BBN universe, should they exist International GW detector networks planned for the future could allow us to explore the equation of state of the universe down to 10^{-16} s after the Big Bang.

Acknowledgments

YG and PS would like to express their gratitude to Géraldine Servant for fruitful discussions that initiated ideas explored in this paper and for providing valuable comments on the draft. We also appreciate the referee's useful remarks. YG thanks Jérôme Vandecasteele for stimulating interactions that contributed to this paper. YG is grateful to the Azrieli Foundation for the award of an Azrieli Fellowship. PS is supported by Spanish AEI-MICINN, PID2020-113334GB-I00 /AEI/10.13039/501100011033 and the Generalitat Valenciana grant PROMETEO/2021/083. LH acknowledges the support of the Science and Technology Facilities Council under Grant ST/T001011/1. LH acknowledges the support of the Institut Pascal at Université Paris-Saclay during the Paris-Saclay Astroparticle Symposium 2022, with the support of the IN2P3 master projet UCMN, the P2IO Laboratory of Excellence (program "Investissements d'avenir" ANR-11-IDEX-0003-01 Paris-Saclay and

JHEP08(2023)196

ANR-10-LABX-0038), the P2I axis of the Graduate School Physics of Université Paris-Saclay, as well as IJCLab, CEA, IPhT, APPEC, and ANR-11-IDEX-0003-01 Paris-Saclay and ANR-10-LABX-0038. AG and PS appreciate the hospitality and partial support from the Mainz Institute for Theoretical Physics (MITP) of the Cluster of Excellence PRISMA$^+$ (Project ID 39083149) during the early-stage work.

A Effects from higher Fourier modes

Due to periodic boundary conditions, any excitation of a cosmic string loop can be expressed as a superposition of Fourier modes with mode numbers k ranging from 1 to a maximum value $k_{\rm max}$, which we now determine. The GW spectrum given by eq. (2.9) assumes the Nambu-Goto (NG) approximation, which neglects the thickness of the string. This approximation breaks down when the string curvature becomes comparable to its thickness. The thickness of the string is estimated to be of the order of the inverse of the U(1)-breaking scalar vacuum expectation value η. Therefore, if the emitted GW frequency $\tilde{f} = 2k/l$ becomes larger than η, the NG approximation is no longer valid. We deduce the highest Fourier mode that is compatible with the NG approximation (see also ref. [124])

$$k_{\rm max} \simeq \frac{\eta L}{2} \simeq \frac{\eta\alpha t}{2} \simeq \frac{\eta\alpha H^{-1}}{4} \simeq 4300 \left(\frac{\alpha}{0.1}\right)\left(\frac{10^{-10}}{G\mu}\right)^{\frac{1}{2}}\left(\frac{\eta}{T}\right)^2, \tag{A.1}$$

where t is the time at which the loop is formed, $L \simeq \alpha t$ is the size of the loop, H is the Hubble parameter, g_* is the effective number of relativistic degrees of freedom, and $T \simeq 1.7\sqrt{M_{\rm pl}H}/g_*^{1/4}$ is the temperature of the radiation-dominated Universe. Trading the temperature T of loop formation for the frequency f of GW today, we obtain

$$k_{\rm max} \simeq \left(\frac{\rm Hz}{f}\right)^2 \left[\frac{g_*(T(f))}{g_*(T_0)}\right]^{\frac{1}{2}} \times \begin{cases} 3.3\cdot 10^{24}\left(\frac{10^{-11}}{G\mu}\right)^{1/2}\left(\frac{50}{\Gamma}\right) & \text{(local)}, \\ 2.3\cdot 10^{21}\left(\frac{\eta}{10^{15}\,\rm GeV}\right)\left(\frac{0.1}{\alpha}\right) & \text{(global)}. \end{cases} \tag{A.2}$$

The maximum mode number $k_{\rm max}$ is estimated to be extremely large, highlighting the importance of properly accounting for the contribution of each mode. In figure 10, we show effects from higher modes on the GW spectrum from CS, assuming a long EMD era. In this work, we account for those effects by summing over a large number of modes ($k_{\rm max} = 10^{12}$).

B High-frequency turning point for global strings

As discussed in section 3.3, the EMD era leads to the global-string GW spectrum with the slope of $-1/3$. This leads to a high-frequency (HF) turning point (beyond which the HF plateau sits) at

$$\begin{aligned} f_{\rm dom} &\simeq f_{\rm dec}\left[\frac{\Omega_{\rm GW}(f_{\rm dec})}{\Omega_{\rm GW}(f_{\rm dom})}\right]^3 = f_{\rm dec}\exp(3N_{\rm MD})\left[\frac{\Omega_{\rm GW}(f_{\rm dec})}{\Omega^{\rm st}_{\rm GW}(f_{\rm dom})}\right]^3, \\ &\simeq f_{\rm dec}\exp(3N_{\rm MD})\mathcal{D}^3(f_{\rm dec}, f_{\rm dom}), \end{aligned} \tag{B.1}$$

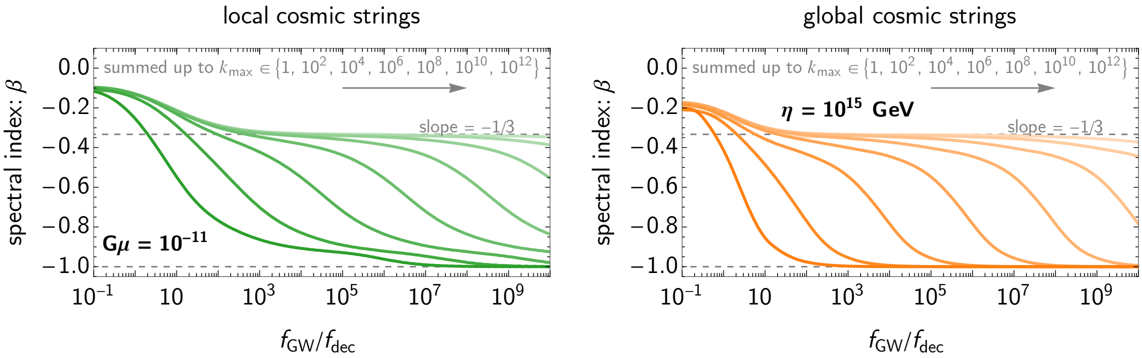

Figure 10. The slopes of cosmic-string GW spectra assuming a long duration ($N_{\mathrm{MD}} = 30$) of EMD era ending at $T_{\mathrm{dec}} = 10^2$ GeV. We can see that the first mode has spectral slope f^{-1}, while summation leads to $f^{-1/3}$ (up to the frequency $k_{\max} f_{\mathrm{dec}}$).

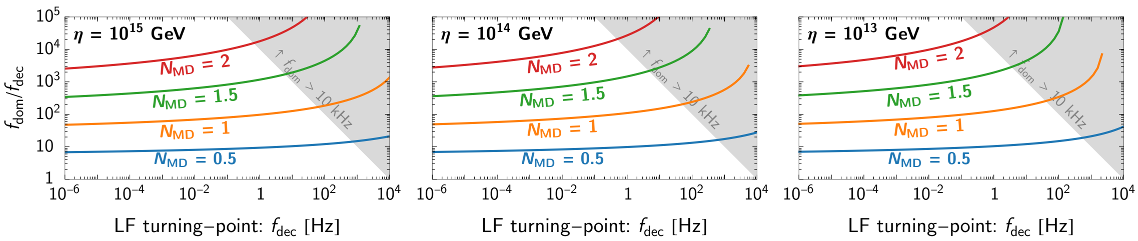

Figure 11. The HF turning-points f_{dom} (solid) of the global cosmic strings depends strongly on the f_{dec} and N_{MD}. The log dependence shifts the turning point higher than the local case (dotted). In the gray region, the HF turning point sits at a frequency higher than 10 kHz and in the ultra-higher frequency regime. This estimates well the numerical results in figure 1.

$$\text{with} \quad \mathcal{D}(f_{\mathrm{dec}}, f_{\mathrm{dom}}) \equiv \frac{\log^3\left[(5.6 \times 10^{30})\left(\frac{\eta}{10^{15}\ \mathrm{GeV}}\right)\left(\frac{1\ \mathrm{mHz}}{f_{\mathrm{dec}}}\right)^2\right]}{\log^3\left[(5.6 \times 10^{30})\left(\frac{\eta}{10^{15}\ \mathrm{GeV}}\right)\left(\frac{1\ \mathrm{mHz}}{f_{\mathrm{dom}}}\right)^2\right]}.$$

The log-dependence term has the 9th power and strongly shifts the HF turning point. Figure 11 shows that the HF turning point of global-string GW, defined in eq. (B.1), sits many order-of-magnitude higher than the LF one, defined in eq. (2.17). Consequently, the HF turning point may lie beyond the detectable range of forthcoming GW interferometers.

C More details on the *knee* feature

C.1 Effects *purely* from the early matter era (unrealistic GW spectrum)

In section 3, we provide the analytic estimates for three features in the double-step GW spectrum from local strings. The g_*–g_{*s} evolution contaminates the effects from the early matter era and complicates the comparison between figure 1 and eqs. (3.5), (3.6), and (3.7). We now consider the effects purely from the early matter era by setting $g_*(T) = g_*(T_0)$ and $g_{*s}(T) = g_{*s}(T_0)$. We show the GW spectrum and its spectral indices in figure 12. The features can be well described by our estimates in eqs. (3.5), (3.6), and (3.7). Furthermore,

JHEP08(2023)196

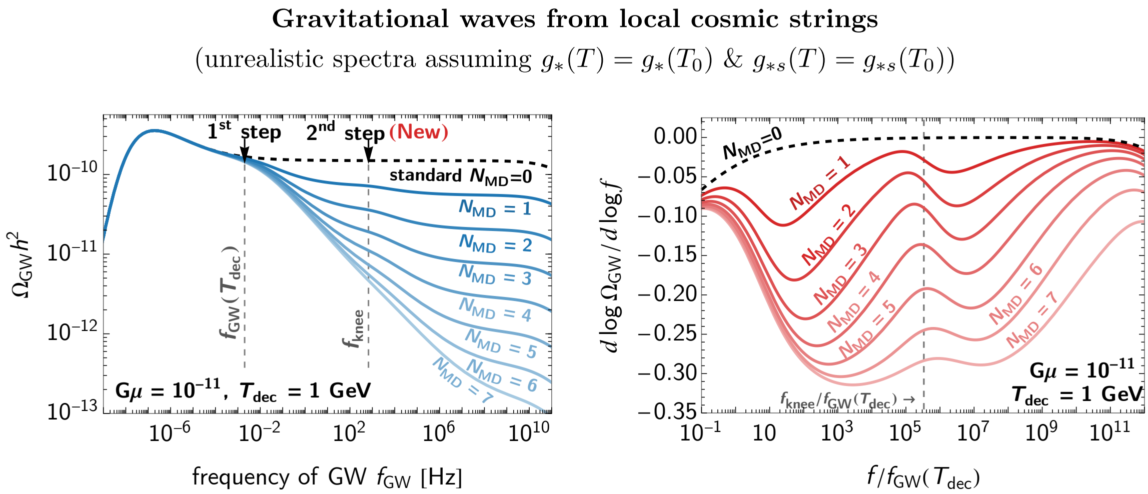

Figure 12. The GW spectra (left) and their spectral indices (right) assume the early matter-domination era with $N_{\rm MD}$ e-folds. The amplitude of the high-frequency plateau and the position of the knee fit well with the analytic estimates in eqs. (3.5), (3.6), and (3.7) with $\mathcal{G} \to 1$.

it can be inferred from figure 12 that the presence of double steps and knee features in the GW spectrum is not caused by the evolution of g_* and g_{*s}, but is solely due to the early matter domination epoch.

C.2 Visibility of the knee feature

As discussed in section 3.4, if the EMD era lasts too long, the knee feature disappears. This happens if the loop lifetime becomes shorter than the EMD duration, i.e., if

$$N_{\rm MD} > \log(\tilde{a}_M/a_i) \simeq 12.28 + \frac{2}{3}\log\left[\left(\frac{\alpha}{0.1}\right)\left(\frac{50}{\Gamma}\right)\left(\frac{10^{-11}}{G\mu}\right)\right], \tag{C.1}$$

where we have used the lifetime of the loops in eq. (2.16) and using $a_{\rm MD} \sim t^{2/3}$.

D Sensitivity curves of GW experiments

The sensitivity of a GW detector is $\Omega_{\rm sens}(f) \equiv 2\pi^2 f^3 S_n(f)/(3H_0^2)$, where $S_n(f)$ is the noise spectral density derived from the correlation of the detector noise signal $n(f)$: $\langle n^*(f)n(f')\rangle \equiv \delta(f-f')S_n(f)$ [100, 252, 253]. The ability of a GW detector to detect a GW signal with energy density $\Omega_{\rm GW}(f)$ is quantified by the signal-to-noise ratio (SNR),

$$\text{SNR} \equiv \sqrt{T\int_{f_{\rm min}}^{f_{\rm max}} df \left[\frac{\Omega_{\rm GW}(f)}{\Omega_{\rm sens}(f)}\right]^2} \quad \text{where } T \equiv \text{ an observation time.} \tag{D.1}$$

The calculation of the SNR can require expensive computations when scanning over the model parameter space. To avoid this, in this paper, we use *the power-law integrated sensitivity curve* [254]. We approximate the GW spectrum as a power-law $\Omega_{\rm GW}(f)$ =

$\Omega_\beta(f/f_\text{ref})^\beta$ with a given spectral index β and reference frequency f_ref. We calculate the GW amplitude Ω_β which gives a certain SNR after an observation time T,

$$\Omega_\beta = \frac{\text{SNR}}{\sqrt{T}} \left(\int_{f_\text{min}}^{f_\text{max}} df \left[\frac{(f/f_\text{ref})^\beta}{\Omega_\text{sens}(f)} \right]^2 \right)^{-1/2}. \tag{D.2}$$

We now sample over all possible spectral index β. One defines the envelope of these curves as the *power-law integrated sensitivity curve*,

$$\Omega_\text{PI}(f;\text{SNR},T) \equiv \max_\beta \left[f^\beta \frac{\text{SNR}}{\sqrt{T}} \left(\int_{f_\text{min}}^{f_\text{max}} df \left[\frac{f^\beta}{\Omega_\text{sens}(f)} \right]^2 \right)^{-1/2} \right]. \tag{D.3}$$

For a detector with noise sensitivity Ω_sens, the observation during time T of a GW signal with amplitude larger than $\Omega_\text{PI}(f;\text{SNR},T)$ has a signal-to-noise ratio $>$ SNR.

The power-law integrated sensitivity curves $\Omega_{PI}(f)$, used in this study, are calculated from the noise spectral density in [97] for ET, [98] for CE, [95] for BBO/DECIGO, [255] for AEDGE, [256] for LISA, and [257] for THEIA. We require SNR $= 10$ with the optimistic observation time of 10 years.[12] For the sensitivity curves of pulsar timing arrays (EPTA, NANOGrav, and SKA), we directly took from [258]. The sensitivity curves of LIGO has been taken into account the improvement from the cross-correlation between multiple detectors [254], where we adopt the noise spectral densities for runs O2, O4, and O5, and the overlap function between the two LIGO detectors from [259]. We fixed the LIGO curves at SNR $= 10$ and the observational time of $T = 268$ days for LIGO O2 and 1 year for LIGO O4 and O5.

References

[1] Planck collaboration, *Planck 2018 results. VI. Cosmological parameters*, *Astron. Astrophys.* **641** (2020) A6 [*Erratum ibid.* **652** (2021) C4] [arXiv:1807.06209] [inSPIRE].

[2] M. Kawasaki, K. Kohri and N. Sugiyama, *Cosmological constraints on late time entropy production*, *Phys. Rev. Lett.* **82** (1999) 4168 [astro-ph/9811437] [inSPIRE].

[3] M. Kawasaki, K. Kohri and N. Sugiyama, *MeV scale reheating temperature and thermalization of neutrino background*, *Phys. Rev. D* **62** (2000) 023506 [astro-ph/0002127] [inSPIRE].

[4] S. Hannestad, *What is the lowest possible reheating temperature?*, *Phys. Rev. D* **70** (2004) 043506 [astro-ph/0403291] [inSPIRE].

[5] A.H. Guth, *The Inflationary Universe: A Possible Solution to the Horizon and Flatness Problems*, *Phys. Rev. D* **23** (1981) 347 [inSPIRE].

[12] The sensitivity is only lost by a small factor when the observation time is reduced by 10%.

[6] A.D. Linde, *A New Inflationary Universe Scenario: A Possible Solution of the Horizon, Flatness, Homogeneity, Isotropy and Primordial Monopole Problems*, Phys. Lett. B **108** (1982) 389 [INSPIRE].

[7] A. Albrecht and P.J. Steinhardt, *Cosmology for Grand Unified Theories with Radiatively Induced Symmetry Breaking*, Phys. Rev. Lett. **48** (1982) 1220 [INSPIRE].

[8] Planck collaboration, *Planck 2018 results. X. Constraints on inflation*, Astron. Astrophys. **641** (2020) A10 [arXiv:1807.06211] [INSPIRE].

[9] Y. Gouttenoire, *Beyond the Standard Model Cocktail*, Springer (2022) [DOI:10.1007/978-3-031-11862-3] [INSPIRE].

[10] J. McDonald, *WIMP Densities in Decaying Particle Dominated Cosmology*, Phys. Rev. D **43** (1991) 1063 [INSPIRE].

[11] T. Moroi and L. Randall, *Wino cold dark matter from anomaly mediated SUSY breaking*, Nucl. Phys. B **570** (2000) 455 [hep-ph/9906527] [INSPIRE].

[12] L. Visinelli and P. Gondolo, *Axion cold dark matter in non-standard cosmologies*, Phys. Rev. D **81** (2010) 063508 [arXiv:0912.0015] [INSPIRE].

[13] A.L. Erickcek, *The Dark Matter Annihilation Boost from Low-Temperature Reheating*, Phys. Rev. D **92** (2015) 103505 [arXiv:1504.03335] [INSPIRE].

[14] A.E. Nelson and H. Xiao, *Axion Cosmology with Early Matter Domination*, Phys. Rev. D **98** (2018) 063516 [arXiv:1807.07176] [INSPIRE].

[15] M. Cirelli, Y. Gouttenoire, K. Petraki and F. Sala, *Homeopathic Dark Matter, or how diluted heavy substances produce high energy cosmic rays*, JCAP **02** (2019) 014 [arXiv:1811.03608] [INSPIRE].

[16] Y. Gouttenoire, G. Servant and P. Simakachorn, *BSM with Cosmic Strings: Heavy, up to EeV mass, Unstable Particles*, JCAP **07** (2020) 016 [arXiv:1912.03245] [INSPIRE].

[17] R. Allahverdi et al., *The First Three Seconds: a Review of Possible Expansion Histories of the Early Universe*, arXiv:2006.16182 [DOI:10.21105/astro.2006.16182] [INSPIRE].

[18] B. Spokoiny, *Deflationary universe scenario*, Phys. Lett. B **315** (1993) 40 [gr-qc/9306008] [INSPIRE].

[19] M. Joyce, *Electroweak Baryogenesis and the Expansion Rate of the Universe*, Phys. Rev. D **55** (1997) 1875 [hep-ph/9606223] [INSPIRE].

[20] P.J.E. Peebles and A. Vilenkin, *Quintessential inflation*, Phys. Rev. D **59** (1999) 063505 [astro-ph/9810509] [INSPIRE].

[21] V. Poulin et al., *Cosmological implications of ultralight axionlike fields*, Phys. Rev. D **98** (2018) 083525 [arXiv:1806.10608] [INSPIRE].

[22] Y. Gouttenoire, G. Servant and P. Simakachorn, *Kination cosmology from scalar fields and gravitational-wave signatures*, arXiv:2111.01150 [INSPIRE].

[23] Y. Gouttenoire, G. Servant and P. Simakachorn, *Revealing the Primordial Irreducible Inflationary Gravitational-Wave Background with a Spinning Peccei-Quinn Axion*, arXiv:2108.10328 [INSPIRE].

[24] R.T. Co et al., *Gravitational wave and CMB probes of axion kination*, JHEP **09** (2022) 116 [arXiv:2108.09299] [INSPIRE].

JHEP08(2023)196

[25] A. Ghoshal, L. Heurtier and A. Paul, *Signatures of non-thermal dark matter with kination and early matter domination. Gravitational waves versus laboratory searches*, *JHEP* **12** (2022) 105 [arXiv:2208.01670] [INSPIRE].

[26] L. Heurtier, A. Moursy and L. Wacquez, *Cosmological imprints of SUSY breaking in models of sgoldstinoless non-oscillatory inflation*, *JCAP* **03** (2023) 020 [arXiv:2207.11502] [INSPIRE].

[27] A.H. Guth and E.J. Weinberg, *A Cosmological Lower Bound on the Higgs Boson Mass*, *Phys. Rev. Lett.* **45** (1980) 1131 [INSPIRE].

[28] E. Witten, *Cosmological Consequences of a Light Higgs Boson*, *Nucl. Phys. B* **177** (1981) 477 [INSPIRE].

[29] P. Creminelli, A. Nicolis and R. Rattazzi, *Holography and the electroweak phase transition*, *JHEP* **03** (2002) 051 [hep-th/0107141] [INSPIRE].

[30] L. Randall and G. Servant, *Gravitational waves from warped spacetime*, *JHEP* **05** (2007) 054 [hep-ph/0607158] [INSPIRE].

[31] T. Konstandin and G. Servant, *Cosmological Consequences of Nearly Conformal Dynamics at the TeV scale*, *JCAP* **12** (2011) 009 [arXiv:1104.4791] [INSPIRE].

[32] B. von Harling and G. Servant, *QCD-induced Electroweak Phase Transition*, *JHEP* **01** (2018) 159 [arXiv:1711.11554] [INSPIRE].

[33] P. Baratella, A. Pomarol and F. Rompineve, *The Supercooled Universe*, *JHEP* **03** (2019) 100 [arXiv:1812.06996] [INSPIRE].

[34] A. Ghoshal and A. Salvio, *Gravitational waves from fundamental axion dynamics*, *JHEP* **12** (2020) 049 [arXiv:2007.00005] [INSPIRE].

[35] I. Baldes, Y. Gouttenoire and F. Sala, *String Fragmentation in Supercooled Confinement and Implications for Dark Matter*, *JHEP* **04** (2021) 278 [arXiv:2007.08440] [INSPIRE].

[36] I. Baldes, Y. Gouttenoire, F. Sala and G. Servant, *Supercool composite Dark Matter beyond 100 TeV*, *JHEP* **07** (2022) 084 [arXiv:2110.13926] [INSPIRE].

[37] A. Dasgupta, P.S.B. Dev, A. Ghoshal and A. Mazumdar, *Gravitational wave pathway to testable leptogenesis*, *Phys. Rev. D* **106** (2022) 075027 [arXiv:2206.07032] [INSPIRE].

[38] F. Ferrer, A. Ghoshal and M. Lewicki, *Imprints of a Supercooled Universe in the Gravitational Wave Spectrum from a Cosmic String network*, arXiv:2304.02636 [INSPIRE].

[39] X. Wong and K.-P. Xie, *Freeze-in of WIMP dark matter*, arXiv:2304.00908 [INSPIRE].

[40] J.D. Barrow, E.J. Copeland and A.R. Liddle, *The Evolution of black holes in an expanding universe*, *Mon. Not. Roy. Astron. Soc.* **253** (1991) 675 [INSPIRE].

[41] K.R. Dienes et al., *Primordial Black Holes Place the Universe in Stasis*, arXiv:2212.01369 [INSPIRE].

[42] K.R. Dienes et al., *Stasis in an expanding universe: A recipe for stable mixed-component cosmological eras*, *Phys. Rev. D* **105** (2022) 023530 [arXiv:2111.04753] [INSPIRE].

[43] B. Carr, K. Kohri, Y. Sendouda and J. Yokoyama, *Constraints on primordial black holes*, *Rept. Prog. Phys.* **84** (2021) 116902 [arXiv:2002.12778] [INSPIRE].

[44] A.M. Green and B.J. Kavanagh, *Primordial Black Holes as a dark matter candidate*, *J. Phys. G* **48** (2021) 043001 [arXiv:2007.10722] [INSPIRE].

JHEP08(2023)196

[45] B.J. Carr, *The Primordial black hole mass spectrum*, *Astrophys. J.* **201** (1975) 1 [INSPIRE].

[46] B.J. Carr and J.E. Lidsey, *Primordial black holes and generalized constraints on chaotic inflation*, *Phys. Rev. D* **48** (1993) 543 [INSPIRE].

[47] P. Ivanov, P. Naselsky and I. Novikov, *Inflation and primordial black holes as dark matter*, *Phys. Rev. D* **50** (1994) 7173 [INSPIRE].

[48] J. Garriga, A. Vilenkin and J. Zhang, *Black holes and the multiverse*, *JCAP* **02** (2016) 064 [arXiv:1512.01819] [INSPIRE].

[49] H. Deng, J. Garriga and A. Vilenkin, *Primordial black hole and wormhole formation by domain walls*, *JCAP* **04** (2017) 050 [arXiv:1612.03753] [INSPIRE].

[50] H. Deng and A. Vilenkin, *Primordial black hole formation by vacuum bubbles*, *JCAP* **12** (2017) 044 [arXiv:1710.02865] [INSPIRE].

[51] A. Kusenko et al., *Exploring Primordial Black Holes from the Multiverse with Optical Telescopes*, *Phys. Rev. Lett.* **125** (2020) 181304 [arXiv:2001.09160] [INSPIRE].

[52] K. Sato, M. Sasaki, H. Kodama and K.-I. Maeda, *Creation of Wormholes by First Order Phase Transition of a Vacuum in the Early Universe*, *Prog. Theor. Phys.* **65** (1981) 1443 [INSPIRE].

[53] K.-I. Maeda, K. Sato, M. Sasaki and H. Kodama, *Creation of De Sitter-schwarzschild Wormholes by a Cosmological First Order Phase Transition*, *Phys. Lett. B* **108** (1982) 98 [INSPIRE].

[54] K. Sato, H. Kodama, M. Sasaki and K.-I. Maeda, *Multiproduction of Universes by First Order Phase Transition of a Vacuum*, *Phys. Lett. B* **108** (1982) 103 [INSPIRE].

[55] H. Kodama, M. Sasaki, K. Sato and K.-I. Maeda, *Fate of Wormholes Created by First Order Phase Transition in the Early Universe*, *Prog. Theor. Phys.* **66** (1981) 2052 [INSPIRE].

[56] H. Kodama, M. Sasaki and K. Sato, *Abundance of Primordial Holes Produced by Cosmological First Order Phase Transition*, *Prog. Theor. Phys.* **68** (1982) 1979 [INSPIRE].

[57] S.D.H. Hsu, *Black Holes From Extended Inflation*, *Phys. Lett. B* **251** (1990) 343 [INSPIRE].

[58] J. Liu et al., *Primordial black hole production during first-order phase transitions*, *Phys. Rev. D* **105** (2022) L021303 [arXiv:2106.05637] [INSPIRE].

[59] K. Kawana, T.H. Kim and P. Lu, *PBH Formation from Overdensities in Delayed Vacuum Transitions*, arXiv:2212.14037 [INSPIRE].

[60] Y. Gouttenoire and T. Volansky, *Primordial Black Holes from Supercooled Phase Transitions*, arXiv:2305.04942 [INSPIRE].

[61] S.W. Hawking, I.G. Moss and J.M. Stewart, *Bubble Collisions in the Very Early Universe*, *Phys. Rev. D* **26** (1982) 2681 [INSPIRE].

[62] I.G. Moss, *Singularity formation from colliding bubbles*, *Phys. Rev. D* **50** (1994) 676 [INSPIRE].

[63] I.G. Moss, *Black hole formation from colliding bubbles*, gr-qc/9405045 [INSPIRE].

[64] M.Y. Khlopov, R.V. Konoplich, S.G. Rubin and A.S. Sakharov, *Formation of black holes in first order phase transitions*, hep-ph/9807343 [INSPIRE].

[65] M. Crawford and D.N. Schramm, *Spontaneous Generation of Density Perturbations in the Early Universe*, *Nature* **298** (1982) 538 [INSPIRE].

[66] C. Gross, G. Landini, A. Strumia and D. Teresi, *Dark Matter as dark dwarfs and other macroscopic objects: multiverse relics?*, JHEP **09** (2021) 033 [arXiv:2105.02840] [INSPIRE].

[67] M.J. Baker, M. Breitbach, J. Kopp and L. Mittnacht, *Detailed Calculation of Primordial Black Hole Formation During First-Order Cosmological Phase Transitions*, arXiv:2110.00005 [INSPIRE].

[68] K. Kawana and K.-P. Xie, *Primordial black holes from a cosmic phase transition: The collapse of Fermi-balls*, Phys. Lett. B **824** (2022) 136791 [arXiv:2106.00111] [INSPIRE].

[69] A. Dolgov and J. Silk, *Baryon isocurvature fluctuations at small scales and baryonic dark matter*, Phys. Rev. D **47** (1993) 4244 [INSPIRE].

[70] A.D. Dolgov, M. Kawasaki and N. Kevlishvili, *Inhomogeneous baryogenesis, cosmic antimatter, and dark matter*, Nucl. Phys. B **807** (2009) 229 [arXiv:0806.2986] [INSPIRE].

[71] N. Kitajima and F. Takahashi, *Primordial Black Holes from QCD Axion Bubbles*, JCAP **11** (2020) 060 [arXiv:2006.13137] [INSPIRE].

[72] K. Kasai, M. Kawasaki and K. Murai, *Revisiting the Affleck-Dine mechanism for primordial black hole formation*, JCAP **10** (2022) 048 [arXiv:2205.10148] [INSPIRE].

[73] J. Martin, T. Papanikolaou and V. Vennin, *Primordial black holes from the preheating instability in single-field inflation*, JCAP **01** (2020) 024 [arXiv:1907.04236] [INSPIRE].

[74] J. Martin, T. Papanikolaou, L. Pinol and V. Vennin, *Metric preheating and radiative decay in single-field inflation*, JCAP **05** (2020) 003 [arXiv:2002.01820] [INSPIRE].

[75] S.G. Rubin, M.Y. Khlopov and A.S. Sakharov, *Primordial black holes from nonequilibrium second order phase transition*, Grav. Cosmol. **6** (2000) 51 [hep-ph/0005271] [INSPIRE].

[76] T. Vachaspati, *Lunar Mass Black Holes from QCD Axion Cosmology*, arXiv:1706.03868 [INSPIRE].

[77] F. Ferrer et al., *Primordial Black Holes from the QCD axion*, Phys. Rev. Lett. **122** (2019) 101301 [arXiv:1807.01707] [INSPIRE].

[78] G.B. Gelmini, A. Simpson and E. Vitagliano, *Catastrogenesis: DM, GWs, and PBHs from ALP string-wall networks*, JCAP **02** (2023) 031 [arXiv:2207.07126] [INSPIRE].

[79] G.B. Gelmini, J. Hyman, A. Simpson and E. Vitagliano, *Primordial black hole dark matter from catastrogenesis with unstable pseudo-Goldstone bosons*, JCAP **06** (2023) 055 [arXiv:2303.14107] [INSPIRE].

[80] S.W. Hawking, *Black Holes From Cosmic Strings*, Phys. Lett. B **231** (1989) 237 [INSPIRE].

[81] A. Polnarev and R. Zembowicz, *Formation of Primordial Black Holes by Cosmic Strings*, Phys. Rev. D **43** (1991) 1106 [INSPIRE].

[82] J. Fort and T. Vachaspati, *Do global string loops collapse to form black holes?*, Phys. Lett. B **311** (1993) 41 [hep-th/9305081] [INSPIRE].

[83] J. Garriga and M. Sakellariadou, *Effects of friction on cosmic strings*, Phys. Rev. D **48** (1993) 2502 [hep-th/9303024] [INSPIRE].

[84] R.R. Caldwell and P. Casper, *Formation of black holes from collapsed cosmic string loops*, Phys. Rev. D **53** (1996) 3002 [gr-qc/9509012] [INSPIRE].

JHEP08(2023)196

[85] J.H. MacGibbon, R.H. Brandenberger and U.F. Wichoski, *Limits on black hole formation from cosmic string loops*, Phys. Rev. D **57** (1998) 2158 [astro-ph/9707146] [INSPIRE].

[86] A.C. Jenkins and M. Sakellariadou, *Primordial black holes from cusp collapse on cosmic strings*, arXiv:2006.16249 [INSPIRE].

[87] J.J. Blanco-Pillado, K.D. Olum and A. Vilenkin, *No black holes from cosmic string cusps*, arXiv:2101.05040 [INSPIRE].

[88] S.W. Hawking, *Black hole explosions*, Nature **248** (1974) 30 [INSPIRE].

[89] S.W. Hawking, *Particle Creation by Black Holes*, Commun. Math. Phys. **43** (1975) 199 [*Erratum ibid.* **46** (1976) 206] [INSPIRE].

[90] C. Keith, D. Hooper, N. Blinov and S.D. McDermott, *Constraints on Primordial Black Holes From Big Bang Nucleosynthesis Revisited*, Phys. Rev. D **102** (2020) 103512 [arXiv:2006.03608] [INSPIRE].

[91] V. Poulin, J. Lesgourgues and P.D. Serpico, *Cosmological constraints on exotic injection of electromagnetic energy*, JCAP **03** (2017) 043 [arXiv:1610.10051] [INSPIRE].

[92] LIGO Scientific et al. collaborations, *A gravitational-wave standard siren measurement of the Hubble constant*, Nature **551** (2017) 85 [arXiv:1710.05835] [INSPIRE].

[93] LIGO Scientific and VIRGO collaborations, *Characterization of the LIGO detectors during their sixth science run*, Class. Quant. Grav. **32** (2015) 115012 [arXiv:1410.7764] [INSPIRE].

[94] LISA collaboration, *Laser Interferometer Space Antenna*, arXiv:1702.00786 [INSPIRE].

[95] K. Yagi and N. Seto, *Detector configuration of DECIGO/BBO and identification of cosmological neutron-star binaries*, Phys. Rev. D **83** (2011) 044011 [*Erratum ibid.* **95** (2017) 109901] [arXiv:1101.3940] [INSPIRE].

[96] M. Punturo et al., *The Einstein Telescope: A third-generation gravitational wave observatory*, Class. Quant. Grav. **27** (2010) 194002 [INSPIRE].

[97] S. Hild et al., *Sensitivity Studies for Third-Generation Gravitational Wave Observatories*, Class. Quant. Grav. **28** (2011) 094013 [arXiv:1012.0908] [INSPIRE].

[98] LIGO Scientific collaboration, *Exploring the Sensitivity of Next Generation Gravitational Wave Detectors*, Class. Quant. Grav. **34** (2017) 044001 [arXiv:1607.08697] [INSPIRE].

[99] B. Allen, *The Stochastic gravity wave background: Sources and detection*, in the proceedings of the *Les Houches School of Physics: Astrophysical Sources of Gravitational Radiation*, (1996), p. 373–417 [gr-qc/9604033] [INSPIRE].

[100] C. Caprini and D.G. Figueroa, *Cosmological Backgrounds of Gravitational Waves*, Class. Quant. Grav. **35** (2018) 163001 [arXiv:1801.04268] [INSPIRE].

[101] P. Simakachorn, *Charting Cosmological History and New Particle Physics with Primordial Gravitational Waves*, Ph.D. thesis, Hamburg University (2022) [INSPIRE].

[102] H.B. Nielsen and P. Olesen, *Vortex Line Models for Dual Strings*, Nucl. Phys. B **61** (1973) 45 [INSPIRE].

[103] T.W.B. Kibble, *Topology of Cosmic Domains and Strings*, J. Phys. A **9** (1976) 1387 [INSPIRE].

JHEP08(2023)196

[104] M. Yamada and K. Yonekura, *Cosmic strings from pure Yang–Mills theory*, *Phys. Rev. D* **106** (2022) 123515 [arXiv:2204.13123] [INSPIRE].

[105] M. Yamada and K. Yonekura, *Cosmic F- and D-strings from pure Yang–Mills theory*, *Phys. Lett. B* **838** (2023) 137724 [arXiv:2204.13125] [INSPIRE].

[106] E.J. Copeland, R.C. Myers and J. Polchinski, *Cosmic F and D strings*, *JHEP* **06** (2004) 013 [hep-th/0312067] [INSPIRE].

[107] G. Dvali and A. Vilenkin, *Formation and evolution of cosmic D strings*, *JCAP* **03** (2004) 010 [hep-th/0312007] [INSPIRE].

[108] J. Polchinski, *Introduction to cosmic F- and D-strings*, in the proceedings of the *NATO Advanced Study Institute and EC Summer School on String Theory: From Gauge Interactions to Cosmology*, (2004), p. 229–253 [hep-th/0412244] [INSPIRE].

[109] M.G. Jackson, N.T. Jones and J. Polchinski, *Collisions of cosmic F and D-strings*, *JHEP* **10** (2005) 013 [hep-th/0405229] [INSPIRE].

[110] S.-H.H. Tye, I. Wasserman and M. Wyman, *Scaling of multi-tension cosmic superstring networks*, *Phys. Rev. D* **71** (2005) 103508 [*Erratum ibid.* **71** (2005) 129906] [astro-ph/0503506] [INSPIRE].

[111] A. Vilenkin, *Gravitational radiation from cosmic strings*, *Phys. Lett. B* **107** (1981) 47 [INSPIRE].

[112] T. Vachaspati and A. Vilenkin, *Gravitational Radiation from Cosmic Strings*, *Phys. Rev. D* **31** (1985) 3052 [INSPIRE].

[113] M.B. Hindmarsh and T.W.B. Kibble, *Cosmic strings*, *Rept. Prog. Phys.* **58** (1995) 477 [hep-ph/9411342] [INSPIRE].

[114] A. Vilenkin and E.P.S. Shellard, *Cosmic Strings and Other Topological Defects*, Cambridge University Press (2000) [INSPIRE].

[115] A. Albrecht and N. Turok, *Evolution of Cosmic Strings*, *Phys. Rev. Lett.* **54** (1985) 1868 [INSPIRE].

[116] D.P. Bennett and F.R. Bouchet, *Evidence for a Scaling Solution in Cosmic String Evolution*, *Phys. Rev. Lett.* **60** (1988) 257 [INSPIRE].

[117] B. Allen and E.P.S. Shellard, *Cosmic string evolution: a numerical simulation*, *Phys. Rev. Lett.* **64** (1990) 119 [INSPIRE].

[118] C.J.A.P. Martins and E.P.S. Shellard, *Extending the velocity dependent one scale string evolution model*, *Phys. Rev. D* **65** (2002) 043514 [hep-ph/0003298] [INSPIRE].

[119] D.G. Figueroa, M. Hindmarsh and J. Urrestilla, *Exact Scale-Invariant Background of Gravitational Waves from Cosmic Defects*, *Phys. Rev. Lett.* **110** (2013) 101302 [arXiv:1212.5458] [INSPIRE].

[120] C.J.A.P. Martins, I.Y. Rybak, A. Avgoustidis and E.P.S. Shellard, *Extending the velocity-dependent one-scale model for domain walls*, *Phys. Rev. D* **93** (2016) 043534 [arXiv:1602.01322] [INSPIRE].

[121] Y. Cui, M. Lewicki, D.E. Morrissey and J.D. Wells, *Cosmic Archaeology with Gravitational Waves from Cosmic Strings*, *Phys. Rev. D* **97** (2018) 123505 [arXiv:1711.03104] [INSPIRE].

[122] Y. Cui, M. Lewicki, D.E. Morrissey and J.D. Wells, *Probing the pre-BBN universe with gravitational waves from cosmic strings*, *JHEP* **01** (2019) 081 [arXiv:1808.08968] [INSPIRE].

[123] N. Ramberg and L. Visinelli, *Probing the Early Universe with Axion Physics and Gravitational Waves*, *Phys. Rev. D* **99** (2019) 123513 [arXiv:1904.05707] [INSPIRE].

[124] Y. Gouttenoire, G. Servant and P. Simakachorn, *Beyond the Standard Models with Cosmic Strings*, *JCAP* **07** (2020) 032 [arXiv:1912.02569] [INSPIRE].

[125] S. Blasi, V. Brdar and K. Schmitz, *Has NANOGrav found first evidence for cosmic strings?*, *Phys. Rev. Lett.* **126** (2021) 041305 [arXiv:2009.06607] [INSPIRE].

[126] S. Datta, A. Ghosal and R. Samanta, *Baryogenesis from ultralight primordial black holes and strong gravitational waves from cosmic strings*, *JCAP* **08** (2021) 021 [arXiv:2012.14981] [INSPIRE].

[127] R. Samanta and F.R. Urban, *Testing super heavy dark matter from primordial black holes with gravitational waves*, *JCAP* **06** (2022) 017 [arXiv:2112.04836] [INSPIRE].

[128] D. Borah, S. Jyoti Das, R. Samanta and F.R. Urban, *PBH-infused seesaw origin of matter and unique gravitational waves*, *JHEP* **03** (2023) 127 [arXiv:2211.15726] [INSPIRE].

[129] G. Barenboim and W.-I. Park, *Gravitational waves from first order phase transitions as a probe of an early matter domination era and its inverse problem*, *Phys. Lett. B* **759** (2016) 430 [arXiv:1605.03781] [INSPIRE].

[130] A. Hook, G. Marques-Tavares and D. Racco, *Causal gravitational waves as a probe of free streaming particles and the expansion of the Universe*, *JHEP* **02** (2021) 117 [arXiv:2010.03568] [INSPIRE].

[131] J. Ellis, M. Lewicki and V. Vaskonen, *Updated predictions for gravitational waves produced in a strongly supercooled phase transition*, *JCAP* **11** (2020) 020 [arXiv:2007.15586] [INSPIRE].

[132] G. Domènech, S. Pi and M. Sasaki, *Induced gravitational waves as a probe of thermal history of the universe*, *JCAP* **08** (2020) 017 [arXiv:2005.12314] [INSPIRE].

[133] M. Giovannini, *Gravitational waves constraints on postinflationary phases stiffer than radiation*, *Phys. Rev. D* **58** (1998) 083504 [hep-ph/9806329] [INSPIRE].

[134] A. Riazuelo and J.-P. Uzan, *Quintessence and gravitational waves*, *Phys. Rev. D* **62** (2000) 083506 [astro-ph/0004156] [INSPIRE].

[135] V. Sahni, M. Sami and T. Souradeep, *Relic gravity waves from brane world inflation*, *Phys. Rev. D* **65** (2002) 023518 [gr-qc/0105121] [INSPIRE].

[136] H. Tashiro, T. Chiba and M. Sasaki, *Reheating after quintessential inflation and gravitational waves*, *Class. Quant. Grav.* **21** (2004) 1761 [gr-qc/0307068] [INSPIRE].

[137] L.A. Boyle and A. Buonanno, *Relating gravitational wave constraints from primordial nucleosynthesis, pulsar timing, laser interferometers, and the CMB: Implications for the early Universe*, *Phys. Rev. D* **78** (2008) 043531 [arXiv:0708.2279] [INSPIRE].

[138] BICEP and KECK collaborations, *Improved Constraints on Primordial Gravitational Waves using Planck, WMAP, and BICEP/Keck Observations through the 2018 Observing Season*, *Phys. Rev. Lett.* **127** (2021) 151301 [arXiv:2110.00483] [INSPIRE].

JHEP08(2023)196

[139] T.L. Smith, M. Kamionkowski and A. Cooray, *Direct detection of the inflationary gravitational wave background*, Phys. Rev. D **73** (2006) 023504 [astro-ph/0506422] [INSPIRE].

[140] K.N. Ananda, C. Clarkson and D. Wands, *The Cosmological gravitational wave background from primordial density perturbations*, Phys. Rev. D **75** (2007) 123518 [gr-qc/0612013] [INSPIRE].

[141] P.D. Lasky et al., *Gravitational-wave cosmology across 29 decades in frequency*, Phys. Rev. X **6** (2016) 011035 [arXiv:1511.05994] [INSPIRE].

[142] M.C. Guzzetti, N. Bartolo, M. Liguori and S. Matarrese, *Gravitational waves from inflation*, Riv. Nuovo Cim. **39** (2016) 399 [arXiv:1605.01615] [INSPIRE].

[143] F. D'Eramo and K. Schmitz, *Imprint of a scalar era on the primordial spectrum of gravitational waves*, Phys. Rev. Research. **1** (2019) 013010 [arXiv:1904.07870] [INSPIRE].

[144] N. Bernal, A. Ghoshal, F. Hajkarim and G. Lambiase, *Primordial Gravitational Wave Signals in Modified Cosmologies*, JCAP **11** (2020) 051 [arXiv:2008.04959] [INSPIRE].

[145] D.I. Dunsky et al., *GUTs, hybrid topological defects, and gravitational waves*, Phys. Rev. D **106** (2022) 075030 [arXiv:2111.08750] [INSPIRE].

[146] M. Berbig and A. Ghoshal, *Impact of high-scale Seesaw and Leptogenesis on inflationary tensor perturbations as detectable gravitational waves*, JHEP **05** (2023) 172 [arXiv:2301.05672] [INSPIRE].

[147] L. Sousa and P.P. Avelino, *Stochastic gravitational wave background generated by cosmic string networks: The small-loop regime*, Phys. Rev. D **89** (2014) 083503 [arXiv:1403.2621] [INSPIRE].

[148] P. Auclair et al., *Probing the gravitational wave background from cosmic strings with LISA*, JCAP **04** (2020) 034 [arXiv:1909.00819] [INSPIRE].

[149] P. Laguna and R.A. Matzner, *Peeling U(1) gauge cosmic strings*, Phys. Rev. Lett. **62** (1989) 1948 [INSPIRE].

[150] A. Vilenkin, *Cosmic string dynamics with friction*, Phys. Rev. D **43** (1991) 1060 [INSPIRE].

[151] C.J.A.P. Martins and E.P.S. Shellard, *String evolution with friction*, Phys. Rev. D **53** (1996) 575 [hep-ph/9507335] [INSPIRE].

[152] C.J.A.P. Martins and E.P.S. Shellard, *Quantitative string evolution*, Phys. Rev. D **54** (1996) 2535 [hep-ph/9602271] [INSPIRE].

[153] B. Allen and E.P.S. Shellard, *Gravitational radiation from cosmic strings*, Phys. Rev. D **45** (1992) 1898 [INSPIRE].

[154] J.J. Blanco-Pillado, K.D. Olum and B. Shlaer, *The number of cosmic string loops*, Phys. Rev. D **89** (2014) 023512 [arXiv:1309.6637] [INSPIRE].

[155] C.-F. Chang and Y. Cui, *Stochastic Gravitational Wave Background from Global Cosmic Strings*, Phys. Dark Univ. **29** (2020) 100604 [arXiv:1910.04781] [INSPIRE].

[156] C.-F. Chang and Y. Cui, *Gravitational waves from global cosmic strings and cosmic archaeology*, JHEP **03** (2022) 114 [arXiv:2106.09746] [INSPIRE].

[157] L. Sousa and P.P. Avelino, *Stochastic Gravitational Wave Background generated by Cosmic String Networks: Velocity-Dependent One-Scale model versus Scale-Invariant Evolution*, Phys. Rev. D **88** (2013) 023516 [arXiv:1304.2445] [INSPIRE].

JHEP08(2023)196

[158] J.J. Blanco-Pillado and K.D. Olum, *Stochastic gravitational wave background from smoothed cosmic string loops*, Phys. Rev. D **96** (2017) 104046 [arXiv:1709.02693] [INSPIRE].

[159] M. Gorghetto, E. Hardy and H. Nicolaescu, *Observing invisible axions with gravitational waves*, JCAP **06** (2021) 034 [arXiv:2101.11007] [INSPIRE].

[160] S. Olmez, V. Mandic and X. Siemens, *Gravitational-Wave Stochastic Background from Kinks and Cusps on Cosmic Strings*, Phys. Rev. D **81** (2010) 104028 [arXiv:1004.0890] [INSPIRE].

[161] A. Vilenkin and T. Vachaspati, *Radiation of Goldstone Bosons From Cosmic Strings*, Phys. Rev. D **35** (1987) 1138 [INSPIRE].

[162] P. Auclair, D.A. Steer and T. Vachaspati, *Particle emission and gravitational radiation from cosmic strings: observational constraints*, Phys. Rev. D **101** (2020) 083511 [arXiv:1911.12066] [INSPIRE].

[163] Particle Data Group collaboration, *Review of Particle Physics*, PTEP **2020** (2020) 083C01 [INSPIRE].

[164] J.N. Moore and E.P.S. Shellard, *On the evolution of Abelian Higgs string networks*, hep-ph/9808336 [INSPIRE].

[165] K.D. Olum and J.J. Blanco-Pillado, *Radiation from cosmic string standing waves*, Phys. Rev. Lett. **84** (2000) 4288 [astro-ph/9910354] [INSPIRE].

[166] J.N. Moore, E.P.S. Shellard and C.J.A.P. Martins, *On the evolution of Abelian-Higgs string networks*, Phys. Rev. D **65** (2002) 023503 [hep-ph/0107171] [INSPIRE].

[167] G. Vincent, N.D. Antunes and M. Hindmarsh, *Numerical simulations of string networks in the Abelian Higgs model*, Phys. Rev. Lett. **80** (1998) 2277 [hep-ph/9708427] [INSPIRE].

[168] M. Hindmarsh, S. Stuckey and N. Bevis, *Abelian Higgs Cosmic Strings: Small Scale Structure and Loops*, Phys. Rev. D **79** (2009) 123504 [arXiv:0812.1929] [INSPIRE].

[169] M. Hindmarsh et al., *Scaling from gauge and scalar radiation in Abelian Higgs string networks*, Phys. Rev. D **96** (2017) 023525 [arXiv:1703.06696] [INSPIRE].

[170] D. Matsunami, L. Pogosian, A. Saurabh and T. Vachaspati, *Decay of Cosmic String Loops Due to Particle Radiation*, Phys. Rev. Lett. **122** (2019) 201301 [arXiv:1903.05102] [INSPIRE].

[171] J.J. Blanco-Pillado and K.D. Olum, *Form of cosmic string cusps*, Phys. Rev. D **59** (1999) 063508 [*Erratum ibid.* **103** (2021) 029902] [gr-qc/9810005] [INSPIRE].

[172] K.D. Olum and J.J. Blanco-Pillado, *Field theory simulation of Abelian Higgs cosmic string cusps*, Phys. Rev. D **60** (1999) 023503 [gr-qc/9812040] [INSPIRE].

[173] J.J. Blanco-Pillado, K.D. Olum and B. Shlaer, *Cosmic string loop shapes*, Phys. Rev. D **92** (2015) 063528 [arXiv:1508.02693] [INSPIRE].

[174] NANOGrav collaboration, *The NANOGrav 12.5 yr Data Set: Search for an Isotropic Stochastic Gravitational-wave Background*, Astrophys. J. Lett. **905** (2020) L34 [arXiv:2009.04496] [INSPIRE].

[175] EPTA collaboration, *Common-red-signal analysis with 24-yr high-precision timing of the European Pulsar Timing Array: inferences in the stochastic gravitational-wave background search*, Mon. Not. Roy. Astron. Soc. **508** (2021) 4970 [arXiv:2110.13184] [INSPIRE].

JHEP08(2023)196

[176] B. Goncharov et al., *On the Evidence for a Common-spectrum Process in the Search for the Nanohertz Gravitational-wave Background with the Parkes Pulsar Timing Array*, *Astrophys. J. Lett.* **917** (2021) L19 [arXiv:2107.12112] [INSPIRE].

[177] J. Antoniadis et al., *The International Pulsar Timing Array second data release: Search for an isotropic gravitational wave background*, *Mon. Not. Roy. Astron. Soc.* **510** (2022) 4873 [arXiv:2201.03980] [INSPIRE].

[178] J. Ellis and M. Lewicki, *Cosmic String Interpretation of NANOGrav Pulsar Timing Data*, *Phys. Rev. Lett.* **126** (2021) 041304 [arXiv:2009.06555] [INSPIRE].

[179] L. Bian et al., *Searching for cosmic string induced stochastic gravitational wave background with the Parkes Pulsar Timing Array*, *Phys. Rev. D* **106** (2022) L101301 [arXiv:2205.07293] [INSPIRE].

[180] Z.-C. Chen, Y.-M. Wu and Q.-G. Huang, *Search for the Gravitational-wave Background from Cosmic Strings with the Parkes Pulsar Timing Array Second Data Release*, *Astrophys. J.* **936** (2022) 20 [arXiv:2205.07194] [INSPIRE].

[181] J.L. Christiansen et al., *Search for Cosmic Strings in the COSMOS Survey*, *Phys. Rev. D* **83** (2011) 122004 [arXiv:1008.0426] [INSPIRE].

[182] Planck collaboration, *Planck 2013 results. XXV. Searches for cosmic strings and other topological defects*, *Astron. Astrophys.* **571** (2014) A25 [arXiv:1303.5085] [INSPIRE].

[183] H. Xiao, L. Dai and M. McQuinn, *Detecting cosmic strings with lensed fast radio bursts*, *Phys. Rev. D* **106** (2022) 103033 [arXiv:2206.13534] [INSPIRE].

[184] M. Hindmarsh, J. Lizarraga, A. Lopez-Eiguren and J. Urrestilla, *Scaling Density of Axion Strings*, *Phys. Rev. Lett.* **124** (2020) 021301 [arXiv:1908.03522] [INSPIRE].

[185] M. Hindmarsh, J. Lizarraga, A. Lopez-Eiguren and J. Urrestilla, *Approach to scaling in axion string networks*, *Phys. Rev. D* **103** (2021) 103534 [arXiv:2102.07723] [INSPIRE].

[186] M. Buschmann, J.W. Foster and B.R. Safdi, *Early-Universe Simulations of the Cosmological Axion*, *Phys. Rev. Lett.* **124** (2020) 161103 [arXiv:1906.00967] [INSPIRE].

[187] M. Buschmann et al., *Dark matter from axion strings with adaptive mesh refinement*, *Nature Commun.* **13** (2022) 1049 [arXiv:2108.05368] [INSPIRE].

[188] M. Gorghetto, E. Hardy and G. Villadoro, *Axions from Strings: the Attractive Solution*, *JHEP* **07** (2018) 151 [arXiv:1806.04677] [INSPIRE].

[189] M. Gorghetto, E. Hardy and G. Villadoro, *More axions from strings*, *SciPost Phys.* **10** (2021) 050 [arXiv:2007.04990] [INSPIRE].

[190] J.A. Dror, H. Murayama and N.L. Rodd, *Cosmic axion background*, *Phys. Rev. D* **103** (2021) 115004 [*Erratum ibid.* **106** (2022) 119902] [arXiv:2101.09287] [INSPIRE].

[191] S. Blasi, V. Brdar and K. Schmitz, *Fingerprint of low-scale leptogenesis in the primordial gravitational-wave spectrum*, *Phys. Rev. Res.* **2** (2020) 043321 [arXiv:2004.02889] [INSPIRE].

[192] D. Borah, S. Jyoti Das and R. Roshan, *Probing high scale seesaw and PBH generated dark matter via gravitational waves with multiple tilts*, arXiv:2208.04965 [INSPIRE].

[193] G.S.F. Guedes, P.P. Avelino and L. Sousa, *Signature of inflation in the stochastic gravitational wave background generated by cosmic string networks*, *Phys. Rev. D* **98** (2018) 123505 [arXiv:1809.10802] [INSPIRE].

JHEP08(2023)196

[194] Y. Cui, M. Lewicki and D.E. Morrissey, *Gravitational Wave Bursts as Harbingers of Cosmic Strings Diluted by Inflation*, Phys. Rev. Lett. **125** (2020) 211302 [arXiv:1912.08832] [INSPIRE].

[195] T. Harada, C.-M. Yoo and K. Kohri, *Threshold of primordial black hole formation*, Phys. Rev. D **88** (2013) 084051 [*Erratum ibid.* **89** (2014) 029903] [arXiv:1309.4201] [INSPIRE].

[196] T. Harada et al., *Primordial black hole formation in the matter-dominated phase of the Universe*, Astrophys. J. **833** (2016) 61 [arXiv:1609.01588] [INSPIRE].

[197] B. Carr et al., *Primordial black hole constraints for extended mass functions*, Phys. Rev. D **96** (2017) 023514 [arXiv:1705.05567] [INSPIRE].

[198] A. Cheek, L. Heurtier, Y.F. Perez-Gonzalez and J. Turner, *Evaporation of primordial black holes in the early Universe: Mass and spin distributions*, Phys. Rev. D **108** (2023) 015005 [arXiv:2212.03878] [INSPIRE].

[199] D.N. Page, *Particle Emission Rates from a Black Hole: Massless Particles from an Uncharged, Nonrotating Hole*, Phys. Rev. D **13** (1976) 198 [INSPIRE].

[200] D.N. Page, *Particle Emission Rates from a Black Hole. 2. Massless Particles from a Rotating Hole*, Phys. Rev. D **14** (1976) 3260 [INSPIRE].

[201] A. Cheek, L. Heurtier, Y.F. Perez-Gonzalez and J. Turner, *Primordial black hole evaporation and dark matter production. II. Interplay with the freeze-in or freeze-out mechanism*, Phys. Rev. D **105** (2022) 015023 [arXiv:2107.00016] [INSPIRE].

[202] J. Auffinger, *Primordial black hole constraints with Hawking radiation—A review*, Prog. Part. Nucl. Phys. **131** (2023) 104040 [arXiv:2206.02672] [INSPIRE].

[203] D. Hooper et al., *Hot Gravitons and Gravitational Waves From Kerr Black Holes in the Early Universe*, arXiv:2004.00618 [INSPIRE].

[204] V. De Luca et al., *The initial spin probability distribution of primordial black holes*, JCAP **05** (2019) 018 [arXiv:1903.01179] [INSPIRE].

[205] M. Calzà, J. March-Russell and J.G. Rosa, *Evaporating primordial black holes, the string axiverse, and hot dark radiation*, arXiv:2110.13602 [INSPIRE].

[206] T. Harada, C.-M. Yoo, K. Kohri and K.-I. Nakao, *Spins of primordial black holes formed in the matter-dominated phase of the Universe*, Phys. Rev. D **96** (2017) 083517 [*Erratum ibid.* **99** (2019) 069904] [arXiv:1707.03595] [INSPIRE].

[207] E. Cotner, A. Kusenko, M. Sasaki and V. Takhistov, *Analytic Description of Primordial Black Hole Formation from Scalar Field Fragmentation*, JCAP **10** (2019) 077 [arXiv:1907.10613] [INSPIRE].

[208] M.M. Flores and A. Kusenko, *Spins of primordial black holes formed in different cosmological scenarios*, Phys. Rev. D **104** (2021) 063008 [arXiv:2106.03237] [INSPIRE].

[209] Y.N. Eroshenko, *Spin of primordial black holes in the model with collapsing domain walls*, JCAP **12** (2021) 041 [arXiv:2111.03403] [INSPIRE].

[210] A. Cheek, L. Heurtier, Y.F. Perez-Gonzalez and J. Turner, *Primordial black hole evaporation and dark matter production. I. Solely Hawking radiation*, Phys. Rev. D **105** (2022) 015022 [arXiv:2107.00013] [INSPIRE].

[211] D. Hooper, G. Krnjaic and S.D. McDermott, *Dark Radiation and Superheavy Dark Matter from Black Hole Domination*, JHEP **08** (2019) 001 [arXiv:1905.01301] [INSPIRE].

JHEP08(2023)196

[212] I. Masina, *Dark matter and dark radiation from evaporating primordial black holes*, *Eur. Phys. J. Plus* **135** (2020) 552 [arXiv:2004.04740] [INSPIRE].

[213] L. Morrison, S. Profumo and Y. Yu, *Melanopogenesis: Dark Matter of (almost) any Mass and Baryonic Matter from the Evaporation of Primordial Black Holes weighing a Ton (or less)*, *JCAP* **05** (2019) 005 [arXiv:1812.10606] [INSPIRE].

[214] J. Auffinger, I. Masina and G. Orlando, *Bounds on warm dark matter from Schwarzschild primordial black holes*, *Eur. Phys. J. Plus* **136** (2021) 261 [arXiv:2012.09867] [INSPIRE].

[215] M.Y. Khlopov, A. Barrau and J. Grain, *Gravitino production by primordial black hole evaporation and constraints on the inhomogeneity of the early universe*, *Class. Quant. Grav.* **23** (2006) 1875 [astro-ph/0406621] [INSPIRE].

[216] R. Allahverdi, J. Dent and J. Osinski, *Nonthermal production of dark matter from primordial black holes*, *Phys. Rev. D* **97** (2018) 055013 [arXiv:1711.10511] [INSPIRE].

[217] O. Lennon, J. March-Russell, R. Petrossian-Byrne and H. Tillim, *Black Hole Genesis of Dark Matter*, *JCAP* **04** (2018) 009 [arXiv:1712.07664] [INSPIRE].

[218] P. Gondolo, P. Sandick and B. Shams Es Haghi, *Effects of primordial black holes on dark matter models*, *Phys. Rev. D* **102** (2020) 095018 [arXiv:2009.02424] [INSPIRE].

[219] I. Baldes, Q. Decant, D.C. Hooper and L. Lopez-Honorez, *Non-Cold Dark Matter from Primordial Black Hole Evaporation*, *JCAP* **08** (2020) 045 [arXiv:2004.14773] [INSPIRE].

[220] N. Bernal and Ó. Zapata, *Dark Matter in the Time of Primordial Black Holes*, *JCAP* **03** (2021) 015 [arXiv:2011.12306] [INSPIRE].

[221] N. Bernal and Ó. Zapata, *Gravitational dark matter production: primordial black holes and UV freeze-in*, *Phys. Lett. B* **815** (2021) 136129 [arXiv:2011.02510] [INSPIRE].

[222] I. Masina, *Dark Matter and Dark Radiation from Evaporating Kerr Primordial Black Holes*, *Grav. Cosmol.* **27** (2021) 315 [arXiv:2103.13825] [INSPIRE].

[223] T. Kitabayashi, *Primordial black holes and scotogenic dark matter*, *Int. J. Mod. Phys. A* **36** (2021) 2150139 [arXiv:2101.01921] [INSPIRE].

[224] N. Bernal, Y.F. Perez-Gonzalez, Y. Xu and Ó. Zapata, *ALP dark matter in a primordial black hole dominated universe*, *Phys. Rev. D* **104** (2021) 123536 [arXiv:2110.04312] [INSPIRE].

[225] N. Bernal and Ó. Zapata, *Self-interacting Dark Matter from Primordial Black Holes*, *JCAP* **03** (2021) 007 [arXiv:2010.09725] [INSPIRE].

[226] N. Bernal, Y.F. Perez-Gonzalez and Y. Xu, *Superradiant production of heavy dark matter from primordial black holes*, *Phys. Rev. D* **106** (2022) 015020 [arXiv:2205.11522] [INSPIRE].

[227] A. Cheek, L. Heurtier, Y.F. Perez-Gonzalez and J. Turner, *Redshift effects in particle production from Kerr primordial black holes*, *Phys. Rev. D* **106** (2022) 103012 [arXiv:2207.09462] [INSPIRE].

[228] A. Arbey et al., *Precision calculation of dark radiation from spinning primordial black holes and early matter-dominated eras*, *Phys. Rev. D* **103** (2021) 123549 [arXiv:2104.04051] [INSPIRE].

[229] N. Bhaumik, A. Ghoshal, R.K. Jain and M. Lewicki, *Distinct signatures of spinning PBH domination and evaporation: doubly peaked gravitational waves, dark relics and CMB complementarity*, *JHEP* **05** (2023) 169 [arXiv:2212.00775] [INSPIRE].

JHEP08(2023)196

[230] NANOGrav collaboration, *The NANOGrav 15 yr Data Set: Search for Signals from New Physics*, *Astrophys. J. Lett.* **951** (2023) L11 [arXiv:2306.16219] [INSPIRE].

[231] G. Servant and P. Simakachorn, *Constraining Post-Inflationary Axions with Pulsar Timing Arrays*, arXiv:2307.03121 [INSPIRE].

[232] K. Inomata et al., *Gravitational Wave Production right after a Primordial Black Hole Evaporation*, *Phys. Rev. D* **101** (2020) 123533 [arXiv:2003.10455] [INSPIRE].

[233] T. Papanikolaou, V. Vennin and D. Langlois, *Gravitational waves from a universe filled with primordial black holes*, *JCAP* **03** (2021) 053 [arXiv:2010.11573] [INSPIRE].

[234] G. Domènech, C. Lin and M. Sasaki, *Gravitational wave constraints on the primordial black hole dominated early universe*, *JCAP* **04** (2021) 062 [*Erratum ibid.* **11** (2021) E01] [arXiv:2012.08151] [INSPIRE].

[235] G. Domènech, V. Takhistov and M. Sasaki, *Exploring evaporating primordial black holes with gravitational waves*, *Phys. Lett. B* **823** (2021) 136722 [arXiv:2105.06816] [INSPIRE].

[236] N. Bhaumik, A. Ghoshal and M. Lewicki, *Doubly peaked induced stochastic gravitational wave background: testing baryogenesis from primordial black holes*, *JHEP* **07** (2022) 130 [arXiv:2205.06260] [INSPIRE].

[237] T. Papanikolaou, C. Tzerefos, S. Basilakos and E.N. Saridakis, *Scalar induced gravitational waves from primordial black hole Poisson fluctuations in f(R) gravity*, *JCAP* **10** (2022) 013 [arXiv:2112.15059] [INSPIRE].

[238] T. Papanikolaou, *Gravitational waves induced from primordial black hole fluctuations: the effect of an extended mass function*, *JCAP* **10** (2022) 089 [arXiv:2207.11041] [INSPIRE].

[239] T. Papanikolaou, C. Tzerefos, S. Basilakos and E.N. Saridakis, *No constraints for f(T) gravity from gravitational waves induced from primordial black hole fluctuations*, *Eur. Phys. J. C* **83** (2023) 31 [arXiv:2205.06094] [INSPIRE].

[240] NANOGrav collaboration, *The NANOGrav 15 yr Data Set: Evidence for a Gravitational-wave Background*, *Astrophys. J. Lett.* **951** (2023) L8 [arXiv:2306.16213] [INSPIRE].

[241] EPTA collaboration, *The second data release from the European Pulsar Timing Array III. Search for gravitational wave signals*, arXiv:2306.16214 [INSPIRE].

[242] D.J. Reardon et al., *Search for an Isotropic Gravitational-wave Background with the Parkes Pulsar Timing Array*, *Astrophys. J. Lett.* **951** (2023) L6 [arXiv:2306.16215] [INSPIRE].

[243] H. Xu et al., *Searching for the Nano-Hertz Stochastic Gravitational Wave Background with the Chinese Pulsar Timing Array Data Release I*, *Res. Astron. Astrophys.* **23** (2023) 075024 [arXiv:2306.16216] [INSPIRE].

[244] EPTA collaboration, *The second data release from the European Pulsar Timing Array: V. Implications for massive black holes, dark matter and the early Universe*, arXiv:2306.16227 [INSPIRE].

[245] C. Caprini et al., *Reconstructing the spectral shape of a stochastic gravitational wave background with LISA*, *JCAP* **11** (2019) 017 [arXiv:1906.09244] [INSPIRE].

[246] Q. Baghi et al., *Uncovering stochastic gravitational-wave backgrounds with LISA*, in the proceedings of the *57th Rencontres de Moriond on Gravitation*, (2023) [arXiv:2307.00649] [INSPIRE].

JHEP08(2023)196

[247] T.B. Littenberg and N.J. Cornish, *Prototype global analysis of LISA data with multiple source types*, Phys. Rev. D **107** (2023) 063004 [arXiv:2301.03673] [INSPIRE].

[248] X. Siemens, X. Martin and K.D. Olum, *Dynamics of cosmic necklaces*, Nucl. Phys. B **595** (2001) 402 [astro-ph/0005411] [INSPIRE].

[249] J.J. Blanco-Pillado and K.D. Olum, *Monopole annihilation in cosmic necklaces*, JCAP **05** (2010) 014 [arXiv:0707.3460] [INSPIRE].

[250] T.W.B. Kibble and T. Vachaspati, *Monopoles on strings*, J. Phys. G **42** (2015) 094002 [arXiv:1506.02022] [INSPIRE].

[251] A. Vilenkin, Y. Levin and A. Gruzinov, *Cosmic strings and primordial black holes*, JCAP **11** (2018) 008 [arXiv:1808.00670] [INSPIRE].

[252] B. Allen and J.D. Romano, *Detecting a stochastic background of gravitational radiation: Signal processing strategies and sensitivities*, Phys. Rev. D **59** (1999) 102001 [gr-qc/9710117] [INSPIRE].

[253] M. Maggiore, *Gravitational wave experiments and early universe cosmology*, Phys. Rept. **331** (2000) 283 [gr-qc/9909001] [INSPIRE].

[254] E. Thrane and J.D. Romano, *Sensitivity curves for searches for gravitational-wave backgrounds*, Phys. Rev. D **88** (2013) 124032 [arXiv:1310.5300] [INSPIRE].

[255] AEDGE collaboration, *AEDGE: Atomic Experiment for Dark Matter and Gravity Exploration in Space*, EPJ Quant. Technol. **7** (2020) 6 [arXiv:1908.00802] [INSPIRE].

[256] LISA Cosmology Working Group collaboration, *Cosmology with the Laser Interferometer Space Antenna*, arXiv:2204.05434 [INSPIRE].

[257] J. Garcia-Bellido, H. Murayama and G. White, *Exploring the early Universe with Gaia and Theia*, JCAP **12** (2021) 023 [arXiv:2104.04778] [INSPIRE].

[258] M. Breitbach et al., *Dark, Cold, and Noisy: Constraining Secluded Hidden Sectors with Gravitational Waves*, JCAP **07** (2019) 007 [arXiv:1811.11175] [INSPIRE].

[259] LIGO Scientific and VIRGO collaborations, *Upper limits on a stochastic gravitational-wave background using LIGO and Virgo interferometers at 600-1000 Hz*, Phys. Rev. D **85** (2012) 122001 [arXiv:1112.5004] [INSPIRE].

JHEP08(2023)196